Precambrian Research 185 (2011) 37–54

Contents lists available at ScienceDirect

Precambrian Research

journal homepage: www.elsevier.com/locate/precamres

The origin of microcontinents in the Central Asian Orogenic Belt: Constraints from paleomagnetism and geochronology

Natalia M. Levashova[a,*], Joseph G. Meert[b], Anatoly S. Gibsher[c], Warren C. Grice[b], Mikhail L. Bazhenov[a]

[a] Geological Institute, Academy of Science of Russia, Pyzhevsky Lane, 7, Moscow 109017, Russia
[b] Department of Geological Sciences, 274 Williamson Hall, Gainesville, FL 32611, USA
[c] Institute of Geology and Mineralogy, Siberian Branch of the Academy of Science of Russia, Koptyug Pr. 3, Novosibirsk 630090, Russia

ARTICLE INFO

Article history:
Received 7 June 2009
Received in revised form 2 December 2010
Accepted 3 December 2010
Available online 13 December 2010

Keywords:
CAOB
Geochronology
Paleomagnetism
Paleolatitude
Late Neoproterozoic

ABSTRACT

The Central Asian Orogenic Belt (CAOB) is widely recognized as a locus of Asia's main growth during the Neoproterozoic–Paleozoic, but its evolution remains controversial. The views on the most enigmatic, late Neoproterozoic to Cambrian, stages are critically dependent on the origin and subsequent kinematics of numerous microcontinents that comprise the structure of Kazakhstan, Tien Shan, Altai and Mongolia.

We report new paleomagnetic data and U–Pb zircon ages from Neoproterozoic volcano-sedimentary rocks from the Lesser Karatau block in central Kazakhstan. The laser ablation U–Pb age of felsic tuff of the Kurgan Fm. is 766 ± 7 Ma. Thermal demagnetization revealed that most studied samples retained a dual-polarity pre-tilting component whose primary origin is supported by a conglomerate test. According these paleomagnetic data, the Lesser Karatau microcontinent was located at a paleolatitude of 34.2 ± 5.3°, N or S, at about 770 Ma. There is only one additional CAOB microcontinent, the Baydaric microcontinent in central Mongolia, for which reliable paleomagnetic data indicate a paleolatitude of 47 ± 14°, N or S, at about 770–805 Ma (Levashova et al., 2010).

Several lines of evidence favor the view that the above CAOB microcontinents were originally parts of two larger domains, thus allowing extrapolation of the above paleomagnetic data to much larger territories, the Kazakhstan and Mongol domains that, in turn, might have belonged to major cratonic areas. A comparison of our paleomagnetic data with those from the larger cratonic nuclei provides first-order constraints on the origins of the CAOB microcontinents. We compare the existing tectonostratigraphic correlations between the Neoproterozoic to early Paleozoic sections of the microcontinents with coeval sections on the margins of Tarim, Australia, South China, Siberia, and North China. This combined analysis excludes a southern hemispheric location for the CAOB microcontinents at 750–800 Ma. Of the several cratons that were located in the northern hemisphere at that time we favor a hypothesis that the Kazakhstan and Mongol domains had originally belonged either to Tarim or South China.

1. Introduction

The Central Asian Orogenic Belt (CAOB) stretches from the Urals via Kazakhstan, the Tien Shan, Altai, and Mongolia to the Pacific. The central part of the belt is located between the East European, Siberian, and Tarim cratons (Fig. 1a) and has a complex tectonic history. Unlike many intra- or peri-continental orogenic belts such as the Urals, Andes, and Appalachians, no prevailing structural trend is observed here. Numerous microcontinents with Precambrian basement and late Neoproterozoic–early Paleozoic clastic–carbonate cover are tectonically juxtaposed with late Neoproterozoic–early Paleozoic subduction-related volcanic complexes, accretionary wedges, and flysch sequences (Mossakovsky et al., 1993). The middle–late Paleozoic structural pattern of the CAOB is dominated by long, strongly curved subduction-related volcanic belts that unconformably overlie the older structures.

Most authors acknowledge the important role of the CAOB in the formation of Eurasia, and a number of contrasting models were proposed to explain its evolution. Notable syntheses (e.g. Zonenshain et al., 1990; Mossakovsky et al., 1993; Didenko et al., 1994; Kheraskova et al., 2003; Khain et al., 2003; Windley et al., 2007) regard the CAOB as an ancient analogue to the setting in the modern western Pacific. These authors argue that the CAOB was formed by the closure of the Paleo-Asian Ocean, where an archipelago of scattered Precambrian microcontinents, oceanic basins and island arcs existed in the late Neoproterozoic–early Paleozoic.

Some models advocate the existence of a long-living volcanic arc system in the paleo-Asian ocean (Sengör and Natal'in, 1996; Puchkov, 2000; Yakubchuk, 2008; Yakubchuk et al., 2002; Stampfli and Borel, 2002). For instance, Sengör and Natal'in (1996) assumed

* Corresponding author. Tel.: +7 495 939 79 72.
E-mail address: namile2007@rambler.ru (N.M. Levashova).

0301-9268/$ – see front matter © 2010 Elsevier B.V. All rights reserved.
doi:10.1016/j.precamres.2010.12.001

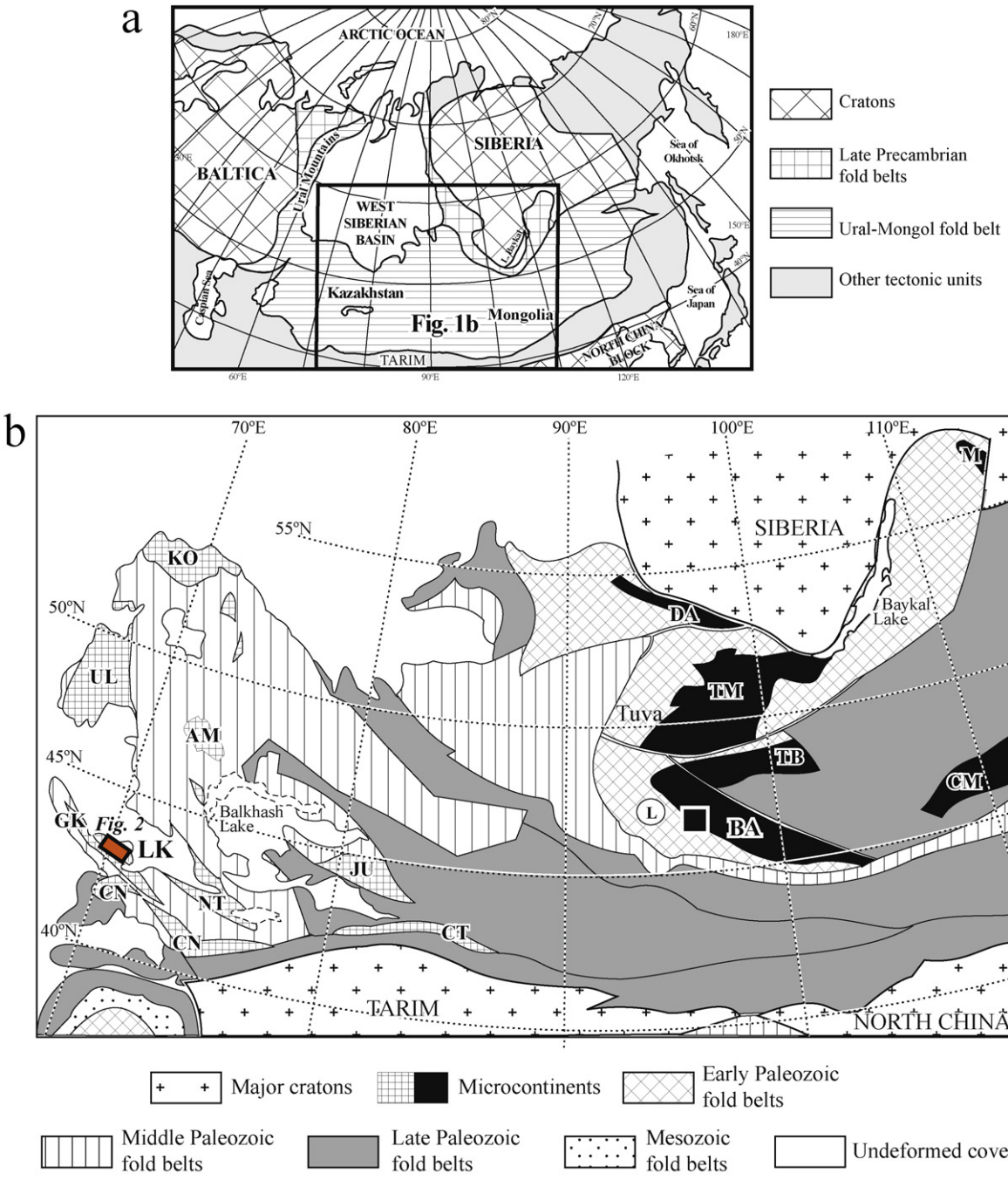

Fig. 1. (a) Location of the Central Asian orogenic belt within Eurasia. (b) Generalized tectonic scheme of the CAOB (the Altaids) and major surrounding units (simplified after Mossakovsky et al., 1993). Microcontinents (cross-hatched in Kazakhstan and black in South Siberia and Mongolia): AM, Aktau-Mointy; BA, Baydaric (or Dzabkhan); CM, Central Mongolian, CN, Chatkal-Naryn; CT, Central Tien Shan; DA, Derbi-Arzubey; GK, Great Karatau; JU, Junggar; KO, Kokchetav; LK, Lesser Karatau; M, Muya; NT, North Tien Shan; TB, Tarbagatay; TM, Tuva-Mongol; UL, Ulutau. Also labeled are the Lake tectonic zone (L) in west Mongolia and the Tuva area in South Siberia. The rectangle outlines the location of Fig. 2. Square denotes the study area on the Baydaric microcontinent (Levashova et al., 2010).

that there was a long, continuous 'Kipchak Arc' connecting Siberia and Baltica in the late Neoproterozoic–early Paleozoic. From the latest Ordovician to the Permian, fragments of the ancient arc were imbricated and gradually amalgamated into a continent-sized domain (Kazakhstan continent).

None of the existing models explains all available data on CAOB geology (e.g. Windley et al., 2007). Biostratigraphic evidence does not adequately discriminate between the models as the spatial distribution of some taxa better match one type of model, whereas other taxa favor a different model (Burtman, 1999). It is possible that the use of paleomagnetic data may offer some resolution between the myriad models proposed for the evolution of the CAOB; however, the present database is too populated for distinguishing between the many models.

If we are to reconstruct the tectonic evolution of the CAOB, then we must begin by establishing the Neoproterozoic–Cambrian history of its development because different choices for the starting point will lead to dissimilar Paleozoic reconstructions. However, these early phases remain both enigmatic and contentious. For instance, the overall stratigraphic similarities between late Neoproterozoic–Cambrian sections on many CAOB microcontinents were noticed decades ago (Ankinovich, 1962; Zubtsov, 1971),

but disparate interpretations were inferred. Some authors assumed that the microcontinents rifted from East Gondwana in the Neoproterozoic and moved as a loose agglomeration across the Paleo-Asian Ocean until collision with either Siberia or each other (Mossakovsky et al., 1993; Didenko et al., 1994; Kheraskova et al., 2003). In contrast, Berzin and Dobretsov (1994) suggested that all these blocks rifted from Siberia in the late Neoproterozoic and re-docked with Siberia in Ediacaran time. Sengör and Natal'in (1996) proposed, albeit implicitly, that all microcontinents rifted from either Siberia or Baltica in the Ediacaran.

Paleomagnetic data from the CAOB microcontinents are invaluable for documenting their origin and subsequent kinematics; however, such data are scarce. Evans et al. (1996) studied carbonates of the early Cambrian Bayan-Gol Formation on the Baydaric (Dzabkhan in other publications) microcontinent in central Mongolia but could only isolate an overprint. The same formation and carbonates of the Ediacaran–Nemakit-Daldynian Tsagan-Oloom Formation were studied by Kravchinsky et al. (2001) who, in addition to the overprint, isolated a dual-polarity component from both formations. These data are highly scattered and are not supported by any field tests, nevertheless, the authors advocate a primary origin for the result. According to Kravchinsky et al. (2001), the Baydaric microcontinent was located near the equator in Ediacaran–early Cambrian times. Kravchinsky et al. (2010) also present paleomagnetic data from Tuva-Mongolia with similar results; namely, a predominant Paleozoic overprint and an inferred ancient magnetization of Ediacaran–Cambrian age. The Ediacaran–Cambrian directions have a shallow inclination suggesting near-equatorial paleolatitudes for Tuva-Mongolia and the Baydaric microcontinents. Minimal paleomagnetic data from Lesser Karatau (Tamdy Series) also indicates a possible low latitude Cambrian-Ordovician position (Pradhan et al., 2009). So far the only other Neoproterozoic paleomagnetic result on the CAOB microcontinents is published by Levashova et al. (2010) who studied Neoproterozoic volcanic rocks from the Baydaric microcontinent (star in Fig. 1b). New paleomagnetic and geochronological data enabled these authors to conclude that about 770–805 Ma ago the Baydaric domain was located at a latitude of $47 \pm 14^{\circ}$, N or S.

We present new paleomagnetic data and U–Pb zircon ages for Neoproterozoic volcano-sedimentary rocks of another CAOB microcontinent, the Lesser Karatau block in central Kazakhstan (Fig. 1b), and discuss tectonic implications of these new results.

2. The Precambrian basement in the CAOB

Precambrian microcontinents within the CAOB cluster mostly in the western part of Central Kazakhstan and to the south of the Siberian craton (Fig. 1b). These microcontinents include the Kokchetav, Ulutau, Karatau-Talas, North Tien Shan, Aktau-Mointy sialic massifs and several smaller blocks. The overall stratigraphic similarities between late Neoproterozoic–Cambrian sections of these microcontinents were noticed decades ago (e.g. Ankinovich, 1962; Zubtsov, 1971). The basement of these massifs typically consists of Paleoproterozoic metamorphic complexes that are overlain by thick piles of Neoproterozoic quartzite and schist with minor carbonates (Degtyarev and Ryazantsev, 2007). The Archean to Paleoproterozoic age of the crystalline basement is demonstrated for several blocks, including the Kokchetav and Ulutau microcontinents, as compiled by Kröner et al. (2007). Detrital zircons with similarly old ages were found in sedimentary sequences from these microcontinents (Kröner et al., 2007). In some microcontinents the available oldest reported ages are much younger: 880 ± 11 Ma in the Aktau-Mointy microcontinent (multigrain zircon age; Kozakov et al., 1993), 780 ± 20 Ma and 816 ± 13 Ma at Greater Karatau (multigrain zircon age; Kozakov et al., 1993; Pradhan, personal communication), 771 ± 17 Ma for Talas (Pradhan, personal communication) and ages ranging from 690 to 720 Ma for Dyzhetym Group in Kyrgyzstan (see Chumakov, 2009a). These younger ages do not preclude older rocks being present in the basement of these domains.

The Neoproterozoic felsic and bi-modal volcanic series of several microcontinents are argued to be coeval and are typically correlated with each other (Chumakov, 2009a,b; Meert et al., in press). Given the age data cited above these correlations seem reasonable (Degtyarev and Ryazantsev, 2007).

From ~750 Ma to ~550 Ma, the geologic record for most microcontinents of the Kazakhstan domain is fragmented. Sedimentary rocks overlie the basement and late Neoproterozoic volcanics on some microcontinents, for instance on the Ulutau microcontinent (Knipper, 1963), but ages are usually inferred on general grounds and often vary from publication to publication. In general, there appears to exist a regional ~100–200 Ma long hiatus, approximately until Ediacaran–Nemakit-Daldynian time (Korolev and Maksumova, 1984; Meert et al., in press).

The geological correlation between microcontinents improves in the terminal Neoproterozoic. The thick carbonate–clastic sequences of latest Neoproterozoic to early Paleozoic age are known on many CAOB microcontinents (Khain et al., 2003 and references therein). The examples include the Karal and Basagin Fms. of the Aktau-Junggar massif and the Tamdy Series of the Lesser Karatau in Kazakhstan. These carbonate–clastic sequences show striking similarities (Ankinovich, 1962; Zubtsov, 1971). The most notable marker horizons are late Neoproterozoic glacial diamictites that are known at one or more stratigraphic levels on several microcontinents (Chumakov, 1978, 2009a; Korolev and Maksumova, 1984) and phosphorite layers that occur at the Ediacaran–Cambrian boundary on some of these blocks (Korolev and Maksumova, 1984; Meert and Lieberman, 2008; Meert et al., in press). Overall the stratigraphic, faunal and lithological similarities led many authors to hypothesize that these blocks originally constituted a continent-size "Kazakhstan" domain (Fig. 1b) with a Paleoproterozoic basement and latest Neoproterozoic to early Paleozoic sedimentary cover (e.g. Degtyarev and Ryazantsev, 2007 and references therein).

Several microcontinents to the south of the Siberian platform (Fig. 1b) can be regarded as remnants of a larger "Mongol" domain, that may have included the Baydaric and Tarbagatay blocks, Tuva-Mongol composite massif (at least the Gargan block), and possibly several smaller blocks. There are several lines of evidence that support a common origin for the Baydaric and Tarbagatay blocks and the Tuva-Mongol massif:

1. The basement formation of the Tuva-Mongol composite massif was completed in the Neoproterozoic with the accretion of continental (Gargan block), oceanic, and island-arc terranes (Kuzmichev, 1996, 2004).
2. The crystalline basement is of similar age in the Baydaric and Tarbagatay blocks (2646 ± 45 Ma, U–Pb on zircon, Kozakov et al., 1993) and in the Gargan block (2450 Ma, U–Pb on zircons, Khain et al., 1995).
3. The last episode of pro-grade metamorphism occurred at 1800–1850 Ma in all these units (Khain et al., 2003).
4. The late Neoproterozoic subduction-related Darkhat-Sarkhoy volcanic series of the Tuva-Mongol massif is similar in age and composition to the Dzabkhan volcanic series of the Baydaric block (Konnikov et al., 1994).
5. Finally, the carbonate–clastic covers of these blocks, (e.g. the Khubsugul Group of the Tuva-Mongol massif and the Tsagan-Oloom Formation of the Baydaric block) that accumulated in a passive-margin environment are similar (Belichenko et al., 1999) and limited paleomagnetic data from these sequences supports the correlation (Kravchinsky et al., 2001, 2010).

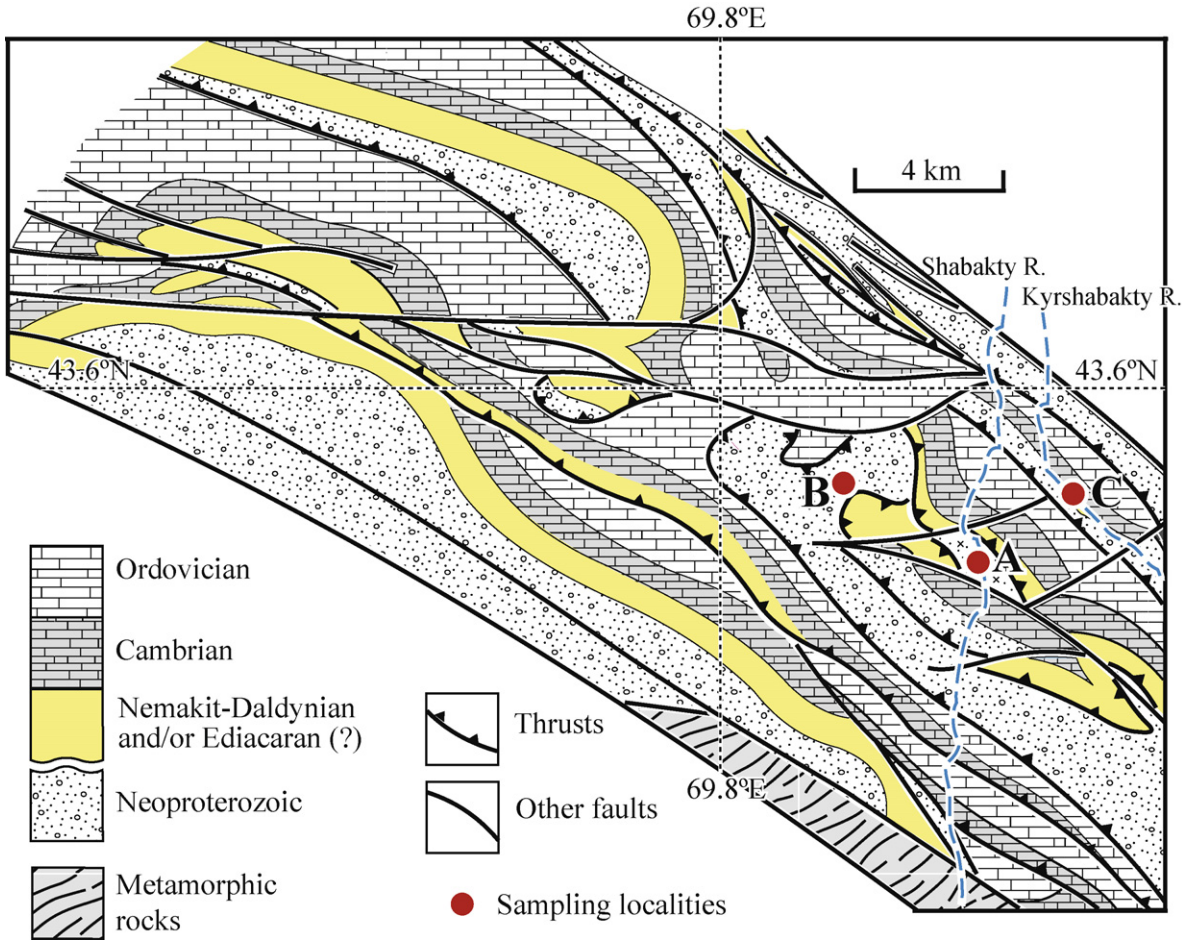

Fig. 2. Schematic geological map of the Lesser Karatau Range. The sampling localities are shown as solid circles and labeled as in the text.

Hence we conclude that the Baydaric and Tarbagatay blocks and the Tuva-Mongol massif are likely to have belonged to the same "Mongol" domain and therefore moved as a single plate in the Precambrian.

3. Geological setting and sampling

Our study concentrated on the Lesser Karatau microcontinent in southern Kazakhstan (Figs. 1b and 2). The most ancient rocks are exposed in a narrow band in the southwestern part of the Lesser Karatau Range (Fig. 2) and consist of thick clastic flysch of the Bolshekaroy Series (Fig. 3). Both series are of presumed Paleoproterozoic age (Sovetov, 1990). However, all contacts are tectonic, and their temporal relationship is uncertain.

The late Neoproterozoic–early Paleozoic sedimentary cover overlies the basement with an angular unconformity and most probably with a large hiatus (Sovetov, 1990). The cover is exposed in a series of NW-striking thrust sheets (Fig. 2). The sedimentary cover is divided into two series (Sovetov, 1990). The older Malokaroy Series is further divided into four formations with conformable contacts between them: (a) redbeds and conglomerates of the Koksu Fm.; (b) arkoses and gritstones of the Aktugay Fm.; (c) black mudstones and cherts of the Chichkan Fm.; (d) volcano-sedimentary rocks of the Kurgan Fm. (Fig. 3).

The rocks of the Malokaroy Series are overlain, with stratigraphic and, locally, weak angular unconformity by the mostly carbonate Tamdy Series which is further divided into several formations (Fig. 3) (Eganov and Sovetov, 1979). The lowermost Kyrshabakty Fm. is represented by a tilloid layer, overlain by pink dolomites, that are, in turn, overlain by a carbonate–terrigenous member (Eganov and Sovetov, 1979). The carbonate Berkuty member of the Chuluctau Fm. overlies the rocks of the Kyrshabakty Fm. with an erosional hiatus. Small shelly fossils (*Protohertzina anabarica Miss.*, *Unguliformis Miss.*) from the Berkuty member correspond to the very end of Nemakit-Daldynian time (zone *Purella antiqua*; Khomentovsky et al., 1998). The carbonates of the Berkuty member are overlain by a phosphorite horizon of the Tommotian age (Missargevsky and Mambetov, 1981) which is, in turn, covered by thick Atdabanian to Middle Ordovician carbonates (Fig. 3) (Mambetov and Repina, 1979; Eganov and Sovetov, 1979). The age of the lowermost Kyrshabakty Fm. remains uncertain. Eganov and Sovetov (1979) assigned a Nemakit-Daldynian age to these rocks; however, the presence of tillites suggests an older Ediacaran age (580 Ma, e.g. Gaskiers) or more probably a Marinoan age (~635 Ma; Meert et al., in press).

Our study concentrated on late Neoproterozoic volcano-sedimentary rocks of the Kurgan Formation that are represented by interlayered pink, red, and green sandstones and siltstones along with silicic tuffs (Fig. 3). The silicic volcanic rocks are mainly ash tuffs and massive pyroclastic flows.

4. U–Pb geochronology

Two samples, K2006-2 and K2006-4, were collected for U–Pb geochronology from a rhyolite tuff sequence at two levels within the Neoproterozoic Kurgan Fm. (Fig. 3).

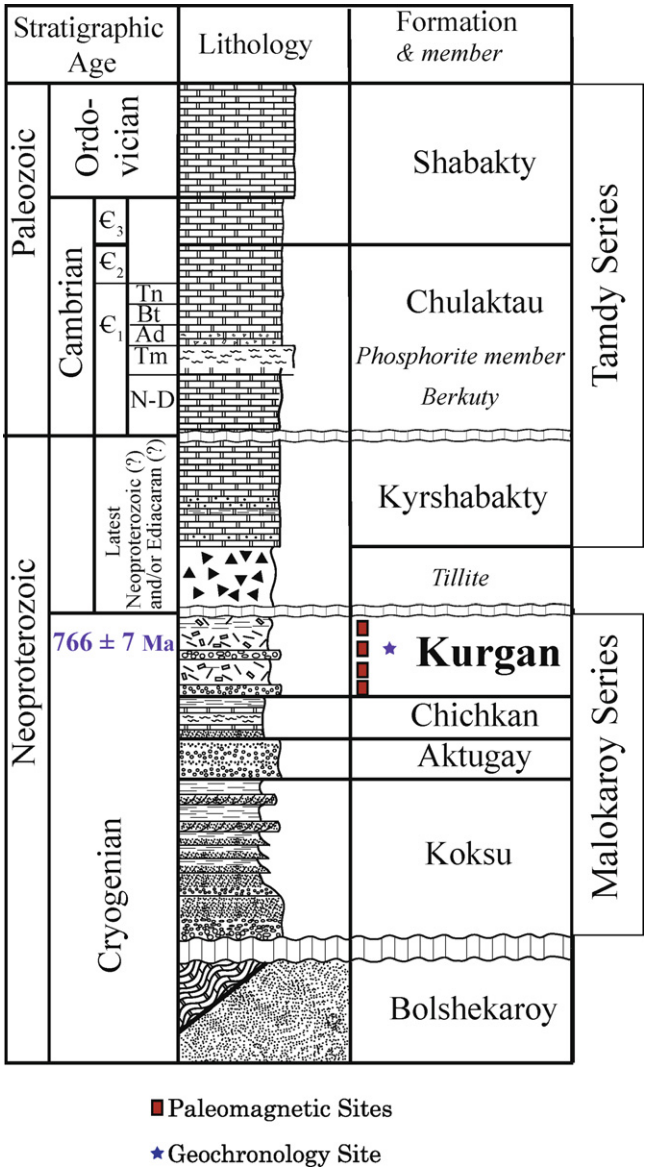

Fig. 3. Schematic stratigraphic column for rocks in the Lesser Karatau microcontinent (thicknesses are arbitrary).

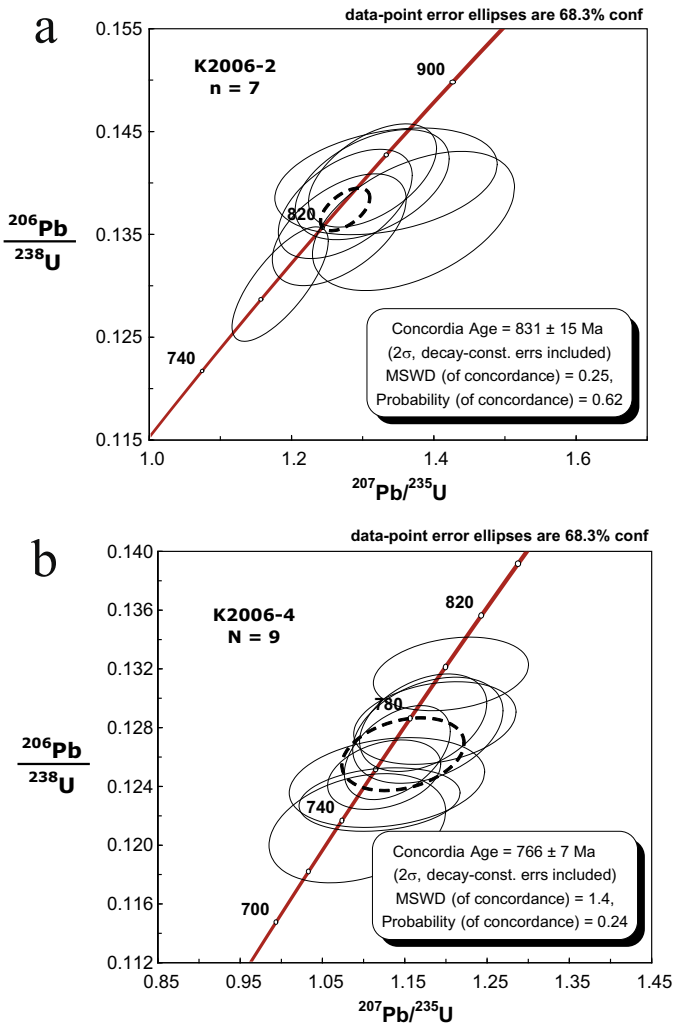

Fig. 4. (a) Concordia diagram for the lowermost tuff yielding an age of 831 ± 15 Ma (2σ). (b) Concordia diagram for the uppermost tuff yielding an age of 766.4 ± 7.2 Ma (2σ).

4.1. Methods

Zircons were extracted from K2006-2 and K2006-4 using standard mechanical crushing, density, and magnetic separation techniques. The least magnetic zircons were then hand-picked under a binocular scope, mounted in epoxy with the external zircon standard FC-1, and polished to expose the zircons. U–Pb isotopic data were obtained from the zircons at the University of Florida using laser ablation multi-collector inductively coupled plasma mass spectrometry (LA-MC-ICP-MS). A New Wave 213 nm ultraviolet laser coupled with a Nu Plasma multi-collector plasma source mass spectrometer was used to ablate individual zircons and to obtain U/Pb isotopic abundances. The LA-MC-ICP-MS analytical equipment and procedure used in this study are described by Simonetti et al. (2005).

The raw U–Pb isotopic ratios obtained from the K2006-2 and K2006-4 zircons by LA-MC-ICP-MS were corrected for laser-induced elemental fractionation and instrumental drift as outlined by Kosler and Sylvester (2003). The analytical errors from the individual zircon unknown and FC-1 standard zircon analyses and true external standard values (TIMS data, Paces and Miller, 1993) were then propagated quadratically for each analysis as described by Horstwood et al. (2003). $^{206}Pb/^{238}U$ ratios were then corrected for common Pb using the "207 method" as summarized by Williams (1998). Common Pb corrected $^{207}Pb/^{235}U$ ratios were then derived from known $^{238}U/^{235}U$ (137.88), the common Pb corrected $^{206}Pb/^{238}U$ ratios, and drift corrected $^{207}Pb/^{206}Pb$ ratios. Conventional concordia diagrams were constructed for these data using the Microsoft Excel spreadsheet add-in program Isoplot v. 3.09a by Ludwig (2004).

4.2. Results

U–Pb geochronology from samples K2006-2 and K2006-4 reveals both Paleoproterozoic–Archean and Neoproterozoic zircons in the Kurgan rhyolite tuff sequence (Fig. 4, Table 1). K2006-2, collected near the base of the tuff sequence, yielded a population of small (~50–100 μm) subhedral zircons that yielded slightly discordant $^{206}Pb/^{238}U$ and $^{207}Pb/^{235}U$ ages ranging from ~2039 to 2790 Ma. Twelve of these zircons are very similar in age and correspond to concordia age of 2032 ± 14 Ma (2σ error). K2006-2 also yielded a population of larger (~150–400 μm) subhedral to euhedral zircons. All seven zircons from the larger population are similar in age and gave a concordia age of 831 ± 15 Ma (2σ error, Fig. 4a).

Table 1
Geochronologic results from Rhyolitic Tuffs.

Grain name	$^{207}Pb/^{235}U^*$	2σ % error*	$^{206}Pb/^{238}U$	2σ % error	RHO (error corr.)	$^{207}Pb/^{235}U$ age	2σ error	$^{206}Pb/^{238}U$ age	2σ error	% Discordance
Paleoproterozoic										
K2006-2-2	6.29492	5.4	0.36299	4.6	0.86	2018	46	1996	78	1
K2006-2-4	6.33664	5.6	0.36908	5.0	0.88	2024	48	2025	86	0
K2006-2-6	6.27429	5.6	0.36454	4.4	0.81	2015	48	2004	76	1
K2006-2-9	6.39292	5.2	0.37263	4.2	0.83	2031	44	2042	74	−1
K2006-2-11	6.36096	5.4	0.37116	4.4	0.80	2027	48	2035	76	0
K2006-2-13	6.44249	6.4	0.37188	4.6	0.73	2038	56	2038	82	0
K2006-2-15	6.49849	5.4	0.37878	4.4	0.82	2046	48	2071	80	−1
K2006-2-19	6.38395	5.2	0.36769	4.6	0.89	2030	46	2019	80	1
K2006-2-20	6.52137	8.2	0.37549	6.4	0.80	2049	70	2055	114	0
K2006-2-26	6.39120	5.4	0.37164	4.6	0.85	2031	48	2037	80	0
Neoproterozoic										
K2006-2-1	1.26609	9.8	0.13543	5.4	0.54	831	56	819	40	1
K2006-2-5	1.18311	7.6	0.13010	5.6	0.75	793	42	788	42	1
K2006-2-3	1.27482	9.8	0.13794	5.2	0.52	835	56	833	40	0
K2006-2-17	1.37103	13.8	0.13628	6.6	0.48	877	80	824	52	6
K2006-2-18	1.31342	9.0	0.14071	4.8	0.52	852	52	849	38	0
K2006-2-23	1.33228	15.6	0.14013	4.8	0.32	860	88	845	38	2
K2006-2-25	1.31256	10.8	0.13981	5.0	0.46	851	62	844	40	1
Neoproterozoic										
K2006-4-1	1.14019	7.4	0.12630	3.4	0.45	773	40	767	24	1
K2006-4-2	1.11935	11.6	0.12317	2.4	0.20	763	62	749	16	2
K2006-4-3a	1.20440	10.4	0.13151	2.6	0.24	803	56	796	18	1
K2006-4-3b	1.17129	8.8	0.12829	3.4	0.39	787	48	778	26	1
K2006-4-4	1.09265	13.0	0.12126	4.0	0.31	750	68	738	28	2
K2006-4-5	1.12785	14.0	0.12429	3.2	0.23	767	74	755	24	1
K2006-4-6	1.12456	8.0	0.12482	2.6	0.31	765	44	758	18	1
K2006-4-8	1.17685	10.2	0.12777	3.8	0.37	790	56	775	28	2
K2006-4-9	1.18537	11.0	0.12826	3.0	0.26	794	60	778	22	2
Other zircons										
K2006-2-8	14.60683	6.6	0.52902	5.8	0.88	2790	62	2737	130	2
K2006-2-10	11.68545	5.2	0.48177	4.6	0.88	2580	48	2535	98	2
K2006-2-12	7.67272	6.0	0.39741	4.2	0.71	2193	54	2157	78	2
K2006-2-22	12.20832	7.8	0.48906	5.6	0.71	2621	74	2567	118	2
K2006-2-24	8.65399	9.0	0.37200	6.6	0.74	2302	84	2039	120	11

Explanation: $^{207}Pb/^{235}U^*$ ratios and errors are calculated from measured $^{207}Pb/^{206}Pb$ and $^{206}Pb/^{238}U$, and known $^{238}U/^{235}U$ (1/137.88). All radiogenic ratios and ages are corrected for instrumental drift. $^{207}Pb/^{235}U$ and $^{206}Pb/^{238}U$ ratios and ages are corrected for U/Pb isotopic fractionation using the intercept method and common lead using the "207" method.

K2006-4, collected from near the middle portion of the rhyolite tuff sequence, yielded a single population of small (~100–200 μm) euhedral zircons. Eight of the nine zircons analyzed from K2006-4 are concordant and gave a concordia age of 766 ± 7 Ma (2σ, Fig. 4b).

The age of the tuff sequence at Lesser Karatau is most likely closer to the younger concordia age of 766 ± 7 Ma. Although the 831 Ma age is concordant, the sample is best described as a reworked tuff and therefore these zircons may be detrital or xenocrystic. The Greater Karatau and Aktau-Mointy blocks contain zircons ranging between 816 and 880 Ma (see Meert et al., in press) and represent a potential source region. Additional support for a ~770 Ma age comes from ages obtained in the Talas Range – considered a stratigraphic equivalent of Lesser Karatau – of 771 ± 17 Ma (Pradhan, personal communication).

5. Paleomagnetic study

5.1. Sampling

The Kurgan Fm. outcrops in the lower parts of many thrust sheets in the Lesser Karatau and dips to the north at various angles (Fig. 2). It is often poorly exposed, affected by penetrative deformation and/or altered. Our sampling concentrated on the Shabakty section (A, 43°30′N, 69°52′E; Fig. 2) where the Kurgan Fm. dips to the north, is nearly continuously exposed and shows no signs of penetrative deformation. These same rocks, with different southeastern and gentle dips, were found at one additional locality (B, 43°33′N, 69°48′E, Fig. 2). In total, we sampled 35 sites from the red sandstones, siltstones, ash tuffs and massive pyroclastic flows from two nearly monoclinal sections with distinctly different bedding attitudes.

Conglomerate beds are abundant in the Neoproterozoic section but always occur below the Kurgan rocks. Nearly all debris in these conglomerates is represented by white quartz and granite. The Kurgan Fm. includes several gritstone members with millimeter-sized debris of the same composition as in the conglomerates below. The only place where greenish-gray cobbles of the Kurgan rocks were found is a limited exposure of tillites of presumed Late Cryogenian age in another thrust sheet to the north of the main section (C in Fig. 2; Meert et al., in press). The Kurgan host rocks at that locality show strong schistosity, but the younger rocks, including the tillite bed as well as the overlying dolomite, are not visibly affected, and we sampled 13 cobbles of the Kurgan tuff from the tillites.

5.2. Methods

A set of samples collected from a one to three meters thick bed or several thinner beds over a similar thickness interval was treated as a single site. The Kurgan rocks proved to be too hard and fragile to permit efficient drilling, and paleomagnetic samples were therefore collected as fist-sized blocks oriented with a magnetic compass. Our convention is to label a site using the letters/numbers of its first sample but with a capital letter at the beginning; for instance, site N4379 contains samples n4379 through to n4386, followed by site N4387, and so forth.

Cubic specimens of 8-cm^3 volume were sawed from the hand samples. The collection was studied in the Paleomagnetic Laboratory of the Geological Institute of the Russian Academy of Sciences

in Moscow. Specimens were heated in a homemade oven with internal residual fields of approximately 10 nT and measured with a JR-4 spinner magnetometer with a noise level of 0.05 mA/m. The specimens were stepwise demagnetized in 15–20 increments up to 680 °C.

Demagnetization results were plotted in orthogonal vector diagrams (Zijderveld, 1967). Visually identified linear trajectories were used to determine directions of magnetic components by Principal Component Analysis (PCA), employing a least-square fit comprising three or more demagnetization steps (Kirschvink, 1980) and anchoring the fitting lines to the origin where appropriate. If complete component separation is not achieved during demagnetization, the common practice is to combine the PCA-calculated sample directions (Kirschvink, 1980) and remagnetization circles for computing site-means of both lower- and higher-temperature components, employing the technique of McFadden and McElhinny (1988).

Paleomagnetic software written by Jean-Pascal Cogné (2003), Randy Enkin (http://gsc.nrcan.gc.ca/dir/index_e.php?id=12377), and Stanislav V. Shipunov was used in the analysis.

5.3. Results

Intensity of the natural remanent magnetization (NRM) of the Kurgan rocks varies from less than 1 mA/m to >100 mA/m. A low-temperature component (LTC) was removed below 200 °C to 300 °C from most samples. The overall mean of this in situ component ($D = 11.1°, I = 62.9°, \alpha_{95} = 6.1°$) is indistinguishable from the present-day field direction for the area ($D = 6°, I = 62°$).

After removal of the present-day field overprint, three distinct demagnetization patterns are observed, sometimes within a site. In some samples, a single component that does not decay to the origin prevails over a temperature interval of up to 570 °C, sometimes to 620–640 °C (Fig. 5a). In a few cases, one intermediate-temperature component (ITC) was succeeded by another that also did not decay to the origin (Fig. 5b); these remanences are labeled as ITC-1 and ITC-2 if both can be identified in a sample. More common are samples where an ITC is followed by a component that shows rectilinear decay to the origin (Fig. 5c–e). This high-temperature component (HTC) is usually resolved above >570 °C or in other cases above 640 °C.

In situ ITC site-means have similar southwesterly declinations, but inclinations vary from moderately steep-and-up to shallow-and-down values, thus resulting in strongly elongated distribution of the data from both fold limbs (Fig. 6a). Upon tilt correction, the scatter increases (Fig. 6b; Table 2). At some sites, strongly elongated distributions of ITC directions were also observed (Fig. 6c and d), whereas unblocking temperatures do not vary from sample to sample. Two limb-mean ITC directions are statistically identical in geographic coordinates and are different after tilt correction (Table 2), and the ITC therefore appears to be a post-folding component (McFadden and Jones, 1981). It is argued that, for the late Paleozoic, the Baltica apparent polar APWP (Torsvik and Cocks, 2005) can serve as a good reference for paleolatitudes for most central Asia, although declinations are often rotated in both senses (Van der Voo et al., 2006). In particular, a characteristic remanence in Upper Permian redbeds from the northern slopes of the Lesser Karatau Range was deflected counterclockwise by ~20° with respect to the Baltica grid (Bazhenov et al., 1995). Applying this same rotation to ITC component brings the ITC directions closer to the reference direction (Fig. 6a).

In some samples, two different ITC components are recognized. These were identified only at sites N4305 and N4363 (Table 2). The strongly elongated distributions at both area and site levels (Fig. 6a, c and d) require an explanation. The ITC directions are more scattered (Table 2) than typical overprint data that tend to be more tightly grouped. One possibility is that the Kurgan rocks have just one ITC with southwest and up directions and the HTC, whereas the directions with southwesterly declinations and shallow inclinations resulted from strong overlapping of unblocking spectra of these two components. The fact that the HTC falls along a great circle connected to the ITC data supports this hypothesis.

Another possibility is that there are two distinct remagnetization components present in the Kurgan rocks. One is likely to be of (late?) Permian age and is the end-member of the observed elongated distribution (Fig. 6a). The second is more problematic, but potentially may be of late Ordovician age for the following reasons. The main folding and thrusting in the Lesser Karatau Range took place in the late Ordovician (Alexeiev, 1990, 1993), and there are coeval granite intrusions in this area. Late Ordovician paleomagnetic results from the western termination of the Tien Shan about 100 km to the northeast of our study area generally have northward declinations and shallow negative inclinations of 10–20°; the north-pointing directions were argued to be of normal polarity (Bazhenov et al., 2003). It is therefore possible that an Ordovician overprint of reverse polarity is present in the Kurgan rocks (diamond in Fig. 6a).

Unfortunately, apart from the limited number of samples and sites where these two overprints can be resolved, there is no way to divide the elongated distribution into the "Permian" and "Late Ordovician" segments (Fig. 6a). Moreover, we are confident that unblocking spectra of different components do overlap in the collection. On the other hand, the elongated distributions for each limb fully overlap in situ and become more distorted and dissimilar after tilt correction. We consider this as an indication that both components are post-folding, consistent with geological data.

The HTC was isolated in many samples in a temperature range that is characteristic of hematite (Fig. 5). In some cases, where unblocking spectra overlap, remagnetization circles were used to isolate the HTC component. Both linear segments and great-circle intersections were combined when computing site means (McFadden and McElhinny, 1988). Most HTC directions are south and down (Fig. 5c and d) although there are a few NW and up directions in the collection (Fig. 5e). At site M1085, both polarities were identified in the lower and upper parts of the approximately two meter thick multi-layer exposure of red sandstones (Table 3). The dispersion of the HTC significantly decreases upon tilt correction (Table 3; Fig. 7a and b), and the best grouping of HTC directions is achieved upon 100% unfolding (Fig. 7c). Out of 17 site-means with south-and-up directions, 14 form a nearly circular cluster, whereas the remaining three are shifted towards the overall ITC mean (gray triangles and inverted triangle, respectively, in Fig. 7b). We suspect that complete component separation was not achieved at these three sites, and they are therefore excluded from the statistical analysis. Limb-mean HTC directions are statistically different in situ and cluster after tilt correction (Table 3; Fig. 7d and e), supporting a pre-folding remanence (McFadden and Jones, 1981). Hence this component predates all deformation that has affected the Kurgan Fm. and may be regarded as primary. The mean HTC inclination of $53.7 \pm 5.4°$ corresponds to a paleolatitude of $34.2 + 5.3°$, N or S.

Most HTC site-mean directions point south and downward and form a tight cluster, whereas some HTC vectors point northwest and upward at four sites (Table 3; Fig. 7a and b). Site-means of *each polarity* are also better grouped after tilt-correction (Table 3), thus rendering the fold test positive for each polarity (McElhinny, 1964). The two polarity-means differ by ~160°, and the critical angle γ_c of ~10° renders the reversal test negative (McFadden and McElhinny, 1990). The imperfect antipodality may be due to the limited number of north-and-up pointing vectors or due to the incomplete removal of secondary postfolding components. We suggest that both factors contribute to the observed pattern and that the presence of a dual-polarity pre-folding magneti-

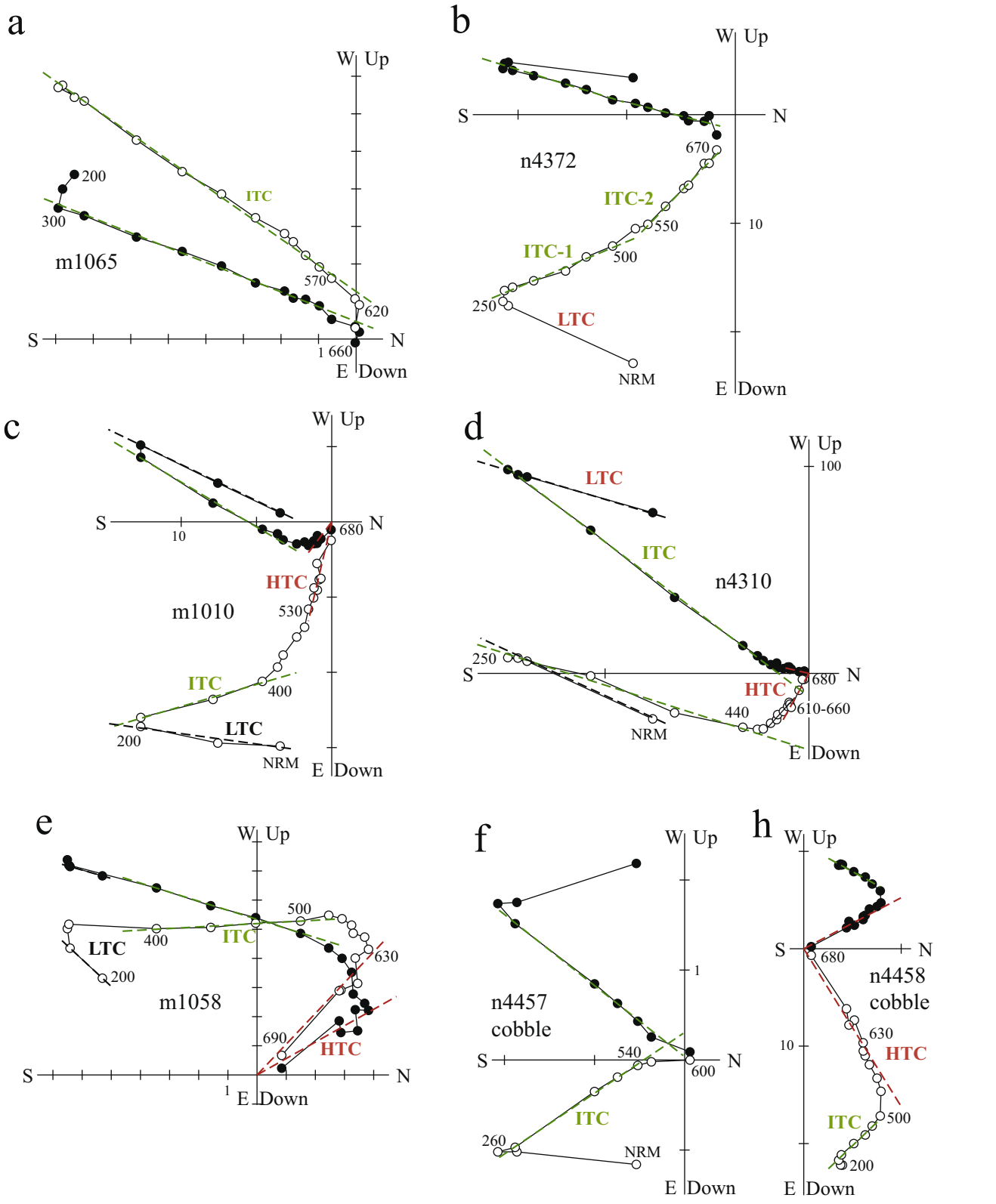

Fig. 5. Representative thermal demagnetization plots for the Kurgan rocks in stratigraphic coordinates. Full (open) circles represent vector endpoints projected onto the horizontal (vertical) plane. Temperature steps are in degrees Celsius. Magnetization intensities are in mA/m. Dashed lines denote isolated components labeled as in the text. NRM values are omitted from some plots for clarity.

zation is a strong indication of a primary remanence in the rocks.

The magnetization components in the cobbles are similarly complex. After removal of the LTC, a single component that does not decay to the origin prevails in most cobbles (Fig. 5f). Its mean in situ direction-falls close to some ITC site-means (Table 2). This remanence clearly fails the conglomerate test and is likely to be a late Paleozoic overprint. Another component with higher unblocking

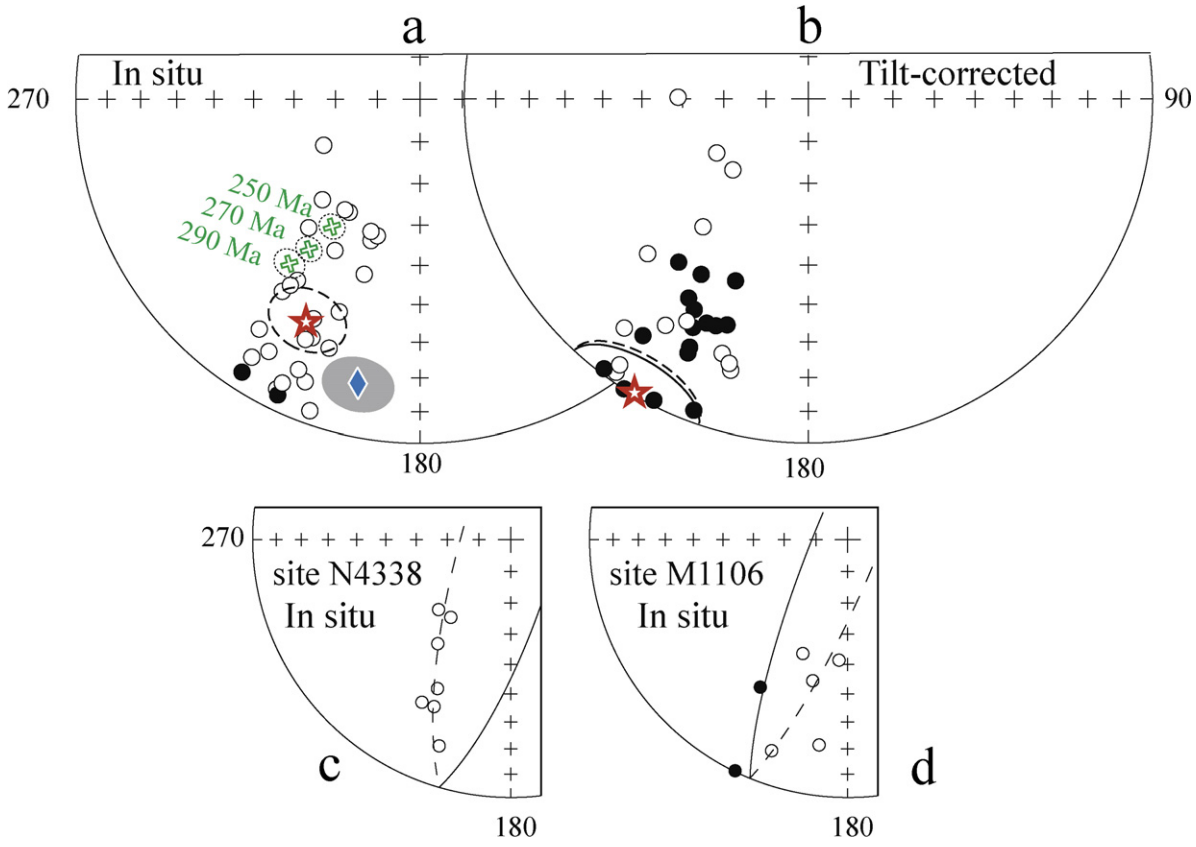

Fig. 6. (a and b) Stereoplots of ITC site-mean directions (circles) in situ (a) and after tilt correction (b); for clarity, confidence circles are not shown. Star is the ITC overall mean with confidence circle (thick line). Crosses are the reference directions for Baltica with confidence circles. Diamond is the Late Ordovician inclination for this area with confidence interval (shaded). (c and d) Elongated distributions of unit ITC directions (small circles) in situ. Solid (open) symbols and solid (dashed) lines are projected onto lower (upper) hemisphere.

temperatures was observed in many cobbles, but a clear isolation of this remanence was possible in only five of the thirteen samples collected (Fig. 5g). The normalized vector-resultant of 0.319 is less than the 95% critical value of 0.7 of the uniformity test (Mardia, 1972), and these five directions are chaotic. Due to the small number of vectors isolated in the cobbles, we cannot confidently conclude a positive conglomerate test, but we argue that the evidence further supports our claim of a primary remanence in the Kurgan Formation.

Paleomagnetic results are summarized as follows. A post-folding LTC of recent age is common. The ITC may be a mixture of two remanences (Permian overprint and the HTC), or a late Ordovician component may be present as well. Irrespective of this ambiguity, the ITC is post-folding and therefore post-dates the Late Ordovician. As noted above, main folding of the Kurgan rocks occurred in the Late Ordovician, although an angular unconformity is observed between the Kurgan Fm. and Ediacaran strata. The late Ordovician directions from the same region are distinct from the HTC data (Figs. 6a and 7b). The south-and-up directions prevail in the HTC data but at least two reversals are stratigraphically bound. Considering all of the paleomagnetic evidence, we suggest that the HTC in the Kurgan rocks is older than the late Ordovician and is likely to be primary in origin.

Reliable Neoproterozoic paleomagnetic data are available only for two of the CAOB microcontinents which are the Baydaric microcontinent in central Mongolia (part of the Mongol domain, Levashova et al., 2010) and the Lesser Karatau microcontinent in Kazakhstan (part of the Kazakhstan domain, this study; Fig. 1b). In the Baydaric microcontinent, Levashova et al. (2010) reported a paleolatitude of $47 \pm 14^\circ$, N or S, for Neoproterozoic (~770–800 Ma) volcanic rocks of the Dzabkhan Fm. According to our new data, the volcano-sedimentary Kurgan Fm, that is the upper member of the late Neoproterozoic cover of the Lesser Karatau block, accumulated at a paleolatitude of $34.2 \pm 5.3^\circ$, N or S, at about 766 ± 7 Ma.

6. Interpretation and discussion

Two new paleomagnetic results with ages of ~775 Ma from South Kazakhstan and from Central Mongolia (Levashova et al., 2010) were obtained. The paleolatitudes of the Lesser Karatau and the Baydaric microcontinents at about 775 Ma by themselves do not give an opportunity to fix these two crustal fragments into a large-scale puzzle. As we are still eager to consider our data on a broader scale, we have to combine the paleomagnetic data with the tectonostratigraphic correlations between the CAOB microcontinents and major cratons.

The tectonostratigraphic correlations between the CAOB microcontinents were discussed earlier along with the observation that many of these microcontinents are floored by Precambrian basement as old as Paleoproterozoic (including zircons recovered in the reworked tuff in our study). This overall similarity allows us to conjecture that most CAOB microcontinents originally belonged to two Madagascar-sized landmasses, the Kazakhstan and Mongol domains.

Most authors accept (or at least, tolerate) the existence of the Precambrian supercontinent Rodinia that supposedly formed at ca. 1100 Ma and broke apart between 800 and 700 Ma (Meert and Torsvik, 2003; Li et al., 2008, and references therein). The period from 800 Ma to about 540 Ma was a time of a major tectonic re-organization – the breakup of Rodinia, followed by the formation of Gondwana (Meert, 2003; Meert and Torsvik, 2004;

Table 2
Intermediate-temperature component data in the Kurgan rocks.

			In situ				Tilt-corrected			
Sites[a]	B°	*N*	*D*°	*I*°	*k*	α_{95}°	*D*°	*I*°	*k*	α_{95}°
M1005	48/48	7/7	209.3	−48.2	43	9.4	215.1	−3.1	31	11.2
M1012	50/48	6/6	204.3	−24.8	92	7.0	205.4	19.3	48	9.8
M1018	49/49	7/6	210.9	−15.6	124	6.0	208.4	30.9	67	8.3
M1025	46/45	7/6	213.1	−11.4	20	15.2	211.0	32.9	26	13.4
M1032[b]	43/32	7/2	215.9	−28.9	–	–	216.7	2.9	–	–
M1039	20/31	7/5	199.1	−54.2	114	7.2	198.7	−22.9	176	5.8
M1048	22/33	8/7	206.3	−6.6	21	13.5	206.8	26.4	21	13.5
M1056	23/26	8/7	200.0	−23.9	72	7.2	200.2	3.9	73	7.1
M1064	11/27	7/7	197.6	−45.6	43	9.3	196.0	−19.0	54	8.3
M1071	36/37	7/7	214.9	−19.6	24	12.5	214.9	17.1	22	13.1
N4305-1	32/41	8/8	224.1	−56.5	38	9.1	218.8	−15.6	36	9.3
N4305-2	28/40	8/4	210.7	−0.5	106	9.0	211.4	39.9	93	9.6
N4313	36/38	8/4	205.7	5.1	190	9.1	201.8	42.4	190	9.1
N4321	46/34	9/6	215.6	−31.8	22	14.6	217.1	1.7	22	14.6
N4330[b]	39/31	8/2	216.3	−38.2	–	–	216.8	−7.2	–	–
N4338	41/31	9/6	214.1	−36.6	24	13.9	215.3	−5.7	24	13.9
N4347	17/35	5/4	199.4	−4.4	31	16.8	199.8	30.8	38	15.1
N4363-1	16/35	8/7	197.3	−55.8	88	6.5	196.7	−20.8	88	6.5
N4363-2	16/35	8/6	191.4	−24.6	42	10.5	191.7	10.3	42	10.5
N4371	22/42	8/8	202.1	−12.3	422	2.7	202.2	29.5	189	4.0
N4379	22/44	9/8	204.2	−14.9	122	5.0	204.4	29.1	138	4.7
N4387	22/44	8/8	205.5	−23.6	92	5.8	205.6	21.0	108	5.3
N4395	30/35	8/7	214.1	−58.1	11	18.7	212.2	−23.2	11	18.7
N4403	36/32	8/8	205.8	−29.8	59	7.3	207.1	1.7	76	6.4
N		(25/20)	207.0	−28.5	16	8.3	207.0	9.0	13	9.4
M1078	158/26	7/7	200.8	−34.2	107	6.0	219.5	−50.1	129	5.5
M1085	159/16	8/5	212.0	−58.2	119	7.1	239.5	−64.7	143	6.4
M1093	146/15	6/5	244.4	−64.7	60	10.2	270.7	−58.9	60	10.2
M1099[b]	144/18	7/6	211.5	14.0	10	21.7	209.1	4.2	11	21.1
M1106[b]	167/19	7/7	203.9	−21.9	6	25.8	212.3	−34.8	6	25.8
N4418	134/16	9/9	214.8	−34.4	91	5.5	226.1	−35.3	91	5.5
N4427	147/14	8/7	213.1	5.9	66	7.5	212.4	0.0	66	7.5
N4435	155/17	8/5	200.3	−56.3	219	5.2	226.8	−65.4	219	5.2
N4443	182/20	8/8	205.8	−9.1	60	7.2	208.7	−27.2	68	6.8
W		(10/7)	211.0	−36.8	8	21.9	224.7	−45.0	9	21.4
Mean		(35/27)	207.9	−30.6	14	7.8	210.4	−4.0	6	12.4
$F_{(2,50)}$ = 3.18			*f* = 0.74				*f* = 20.5			
Cobbles	26/90	13/11	220.8	−49.1	14	12.5	218.5	39.2	14	12.5

Comments: N and W are the sections with the dips to the northeast and southeast, respectively (Fig. 2); the entries N4305-2 and N4363-2 were not used in computation of the overall mean and are not shown in Fig. 5a and b. *B* is the site's azimuth of dip/dip angle; *N* is the number of samples (sites) studied/accepted; *D*, declination; *I*, inclination; *k*, concentration parameter; α_{95}, radius of 95% confidence circle (Fisher, 1953).

[a] Not shown are the sites where no ITC is isolated or ITC directions are very scattered.

[b] Excluded from computation of the overall mean because of small statistics or low precision.

Meert and Lieberman, 2008). For instance, Hoffman (1991) suggested that the break-up of Rodinia at about 800–700 Ma involved fragmentation around Laurentia with continental fragments moving away from Laurentia and colliding on the other side of the Earth to form Gondwana. Meert (2003) argued that West Gondwana was largely assembled by ca. 600 Ma (with the exception of Kalahari and perhaps some minor terranes), whereas Australia–East Antarctica, India, eastern Africa and Kalahari were still separated by the oceanic basins (see also Gregory et al., 2009). Gondwana was finally amalgamated by ca. 540–530 through the docking of India to Australia–East Antarctica (Meert, 2003). However, due to the scarcity of paleomagnetic data, more accurate kinematics of this sequence of events are poorly defined. Moreover, the orientation and location of the landmasses that comprised Rodinia remain highly controversial (Meert and Torsvik, 2003), and it is thus premature to compare data from the Kazakhstan and Mongol domains with different models of Rodinia.

As an alternative to a Rodinia comparison, we prefer to compare the observed paleolatitudes from the Kazakhstan and Mongol domains to those recalculated from 750 to 800 Ma paleomagnetic poles for other larger cratons. Note that neither paleomagnetic poles nor declinations can be used for the Mongol and Kazakhstan regions because subsequent rotations within the mobile CAOB have distorted them "beyond recognition". Moreover, because of the hemispheric ambiguity of paleomagnetic data, we have to examine both polarity options.

If the southern hemisphere option is chosen (downward-and-south pointing directions in Fig. 7 are reverse), the Kazakhstan and Mongol domains are placed at mid-southern latitudes in the vicinity of western Gondwana cratons (West Africa and Amazonia) or amidst the Brasiliano Ocean. If we adhere to the northern hemisphere option (downward-and-south pointing directions in Fig. 7 are normal), the paleolatitudes of these microcontinents are compatible with those for Australia, Tarim, South China, India, and North China, whereas Siberia and Laurentia occupied lower latitudes (Fig. 8, Table 4). The data scarcity for both microcontinents and cratons does not permit a more definitive choice, and further progress requires a review of tectonostratigraphic correlations between the CAOB microcontinents and major cratons.

The Neoproterozoic to early Paleozoic sections of the CAOB microcontinents show many similarities not only with each other but also with coeval sections on the margins of Tarim, Australia, South China, and, to a lesser degree, Siberia and North China (Korolev and Maksumova, 1984; Esakova and Zhegallo, 1996; Khomentovsky, 1996; Li et al., 2002; Khain et al., 2003; Xiao et al., 2004; Chumakov, 2009b). The geological arguments for these cor-

Table 3
High-temperature component data in the Kurgan rocks.

			In situ				Tilt corrected			
Sites[a]	B	*N*	*D*°	*I*°	*k*	a_{95}°	*D*°	*I*°	*k*	a_{95}°
M1005	48/48	7/7	202.8	20.9	16	15.8	176.0	59.9	23	13.1
M1012	50/48	6/6	203.8	12.4	94	7.0	184.2	52.9	113	6.3
M1018	49/49	7/6	16.0	−24.5	11	21.1	344.2	−58.2	14	19.2
M1025	46/45	7/5	211.5	24.3	31	15.9	191.9	66.3	46	13.0
M1032	43/32	7/5	197.9	30.6	78	9.4	180.1	57.7	78	9.4
M1039[b]	20/31	7/3	190.8	−78.6	59	19.0	196.9	−47.7	49	23.2
M1048	19/33	8/5	202.1	17.2	58	10.8	203.5	50.5	51	11.6
M1056	23/26	8/4	341.9	−24.8	69	11.1	328.5	−43.0	56	12.4
M1064	11/27	7/4	178.3	30.6	35	21.4	171.3	56.2	50	17.8
N4305	34/42	8/8	194.8	13.6	59	7.3	183.0	51.9	76	6.5
N4313	36/38	8/4	205.7	5.1	190	9.1	201.8	42.4	190	9.1
N4330	39/31	8/4	200.3	31.3	82	10.8	186.4	59.6	82	10.8
N4371	22/41	8/8	188.9	13.9	234	3.8	180.4	53.7	503	2.6
N4379	21/44	9/8	190.1	2.6	113	5.2	185.3	45.6	124	5.0
N4387	22/44	8/8	187.9	5.3	118	5.2	180.9	48.0	118	5.2
N		(25/14)	194.6	18.7	28	7.6	181.3	54.1	53	5.5
M1078	156/26	7/7	346.5	−64.1	110	6.2	342.0	−38.7	63	8.2
M1085-N	145/15	3/3	221.8	66.4	44	18.7	195.1	59.6	44	17.3
M1085-R	160/16	5/5	311.1	−71.9	59	10.4	324.0	−56.7	61	10.1
M1099	149/18	7/6	213.5	55.5	340	3.8	195.2	45.0	270	4.3
M1106§	167/19	7/5	208.1	49.2	136	7.1	197.9	33.7	108	7.9
N4427§	146/15	8/7	214.6	38.8	73	7.1	205.0	32.3	77	6.9
N4443§	185/22	8/8	217.5	49.0	84	6.5	208.9	29.3	83	6.5
W		(10/7)	203.9	59.1	19	14.3	189.6	44.2	16	15.8
W1		(10/4)	189.8	68.4	22	20.2	174.0	52.0	20	21.2
Mean		(35/21)	196.3	31.8	11	9.9	184.1	50.9	28	5.9
Mean1		(35/18)	194.2	29.2	10	11.5	179.6	53.7	41	5.4
$F_{(2,32)}$ = 3.29			*f* = 28.4				*f* = 0.44			
Reverse		(4)	351.2	−48.3	8	36.1	334.8	−49.4	49	13.2
Normal		(14)	198.6	23.5	16	10.4	187.2	53.9	83	4.4

W and Mean are calculated for all data; W1 and Mean1 are computed without three site-means marked with § (see text for discussion). Polarity assignments are arbitrary. Other notation is as in Table 2.

[a] Not shown are the sites where no HTC is isolated or HTC directions are very scattered.
[b] Anomalous direction is excluded from computation of the overall mean.

relations are: (1) the cratons have Archean to Paleoproterozoic basement; (2) volcanic series that are broadly coeval with the Neoproterozoic volcanic series of the CAOB microcontinents are known in South China, Tarim and Australia; (3) the cratons have the late Neoproterozoic–Cambrian carbonate–clastic sedimentary cover that show striking stratigraphic similarities to the sedimentary cover of the microcontinents; (4) late Neoproterozoic glacial deposits at one or more stratigraphic levels are found on all of these cratons (Meert et al., in press; Chumakov, 2009a).

On the South China craton, rift-related bimodal magmatism was described at 830–795 Ma and 780–745 Ma (Li et al., 2002). The late Neoproterozoic–Cambrian carbonate–clastic sequences of the Yangtze area show striking similarities to the sedimentary cover of the CAOB microcontinents, in particular to the Baydaric and Tuva-Mongol blocks in the Mongol domain, and have up to three Neoproterozoic glacial intervals (Khomentovsky, 1996).

Probably best documented are the correlations between the Kazakhstan microcontinents and the Tarim craton where detailed descriptions can be found (e.g. Chumakov, 2009b). Here, we mention that (1) the 820–750 Ma bimodal volcanic rocks in Tarim (Lu et al., 2008) may correlate with the Neoproterozoic felsic and bi-modal volcanic series of many CAOB microcontinents; (2) the late Neoproterozoic–Cambrian carbonate–clastic sequence of the Quruqtagh range on Tarim is similar to coeval sections of the Kazakhstan domain and has up to three Neoproterozoic glacial intervals (Xiao et al., 2004; Chumakov, 2009b). The above evidence allowed Khain et al. (2003) to propose that a single Kazakhstan-Tarim continent existed in the Neoproterozoic–Cambrian.

The Neoproterozoic to early Paleozoic sections of northwestern Australia also show some similarities with the coeval CAOB sections. However, Chumakov (2009b) considers stratigraphic similarities between the Australian sections and those of the CAOB microcontinents to be less convincing. The Neoproterozoic volcanic series of the CAOB microcontinents are broadly coeval the ca. 820–800 Ma lamprophyre dykes and kimberlite pipes in the Kimberley craton of western Australia (Pidgeon et al., 1989) and the 755 Ma Mundine Well dyke swarm in the northwestern Pilbara craton (Wingate and Giddings, 2000), but differ in character. The Australian igneous activity is mafic/ultramafic whereas magmatism in the CAOB is more felsic or bi-modal. While these differences may simply reflect distinct positions within the same tectonic setting, we feel that they do not offer strong evidence of close affinity between the two blocks. The sedimentary sections of the Kimberley region of northwestern Australia have up to three Neoproterozoic glacial intervals (Li et al., 1996), but much of the remaining stratigraphy is distinct from the CAOB sequences, but probably these facts do not give us enough ground for the correlations with the CAOB microcontinents.

In North China, magmatic rocks ranging in age from 1100 to 700 Ma are rare (Zhao et al., 2006; Lu et al., 2008). Late Neoproterozoic glacial diamictites are known here at more than one stratigraphic level. The carbonate sequences of North China, however, can be correlated only with the upper part of the sedimentary cover of Tarim, South China and the CAOB microcontinents (Chumakov, 2009b).

We know of no studies where geological similarities between Neoproterozoic sections of India and the CAOB microcontinents were proposed or validated, although depositional sequences of the Krol-Tal Belt (Lesser Himalayas) might be a potential candidate for Late Neoproterozoic–Cambrian comparison (Shanker et al., 2004)

Table 4
Selected paleomagnetic poles.

No	Rock unit	Age (Ma)	Pole		A_{95}°	Lat°	Reference
			Φ°	Λ°			
India/Seychelles							
2	Malani rhyolites (IND)	761 ± 10	75	71	10	39N–23N	Torsvik et al. (2001a)
3	Mahe granites (SEY)[e]	755 ± 1	77	23	2	32N–15N	Torsvik et al. (2001b)
4	Mahe dykes (SEY)[e]	750 ± 3	80	79	16	34N–18N	Torsvik et al. (2001b), Hargraves and Duncan (1990)
Australia							
5	Hussar Formation	800–760	62	86	10	3N–19S	Pisarevsky et al. (2007)
6	Mundine dykes	755 ± 3	45	135	4	31N–8N	Wingate and Giddings (2000)
7	Walsh Tillite	750–770	22	102	14	44N–19N	Li (2000)
	Yaltipena Formation[c]	620–630	44	173	8	27N–5N	Sohl et al. (1999)
	Elatina Formation[c]	600–620	39	186	9	26N–1N	Sohl et al. (1999)
	Brachina Formation[c]	~580	33	148	16	44N–20N	McWilliams and McElhinny (1980)
	Lower Arumbera/Pertataka Formation[c]	~570	44	162	10	30N–7N	Kirschvink (1978)
	Upper Arumbera SS[c]	~550	46	157	4	30N–6N	Kirschvink (1978)
	Todd River	~530	43	160	7	32N–9N	Kirschvink (1978)
South China							
8	Xiaofeng dykes	807 ± 10	14	91	11	~69N	Li et al. (2004)
9	Liantuo Formation	748 ± 12	4	161	13	~37N	Evans et al. (2004)
10	Nantuo Formation[d]	~740	0	151	5	~43N	Rui and Piper (1997)
	Meishucun Formation[d]	~525	9	31	10	~14N	Lin et al. (1985)
	Tianheban Formation[d]	~511	−7	10	23	~12S	Lin et al. (1985)
	Hetang Formation[d]	~511	−38	16	17	~18S	Lin et al. (1985)
North China							
11	Nanfen Formation	800–780	−16	121	11	~39N	From Zhang et al. (2006)
	Mean pole	~700	−43	107	6	~11N	From Zhang et al. (2006)
	Donjia Formation, Lushan	~650	−61	97	7	~8S	From Zhang et al. (2006)
Tarim							
12	Aksu Dykes	807 ± 12	19	128	6	~43N	Chen et al. (2004)
13	Baiyixi Formation	~740	17	194	4	6S	Huang et al. (2005)
Laurentia							
14	Galeros Formation	780–820	−2	163	6	21N–25S	Weil et al. (2004)
15	Wyoming dykes	782 ± 8; 785 ± 8	13	131	4	23N–36S	Harlan et al. (1997)
16	Tsezotene sills and dykes	779 ± 2	2	138	5	16N–34S	Park et al. (1989)
17	Kwagunt Formation	742 ± 6	18	166	7	41N–6S	Weil et al. (2004)
18	Natkusiak Formation	723 ± +4/−2	6	159	6	27N–20S	Palmer et al. (1983), Heaman et al. (1992)
19	Franklin dykes	723 ± +4/−2	5	163	5	27N–19S	Heaman et al. (1992), Park (1994)
	Long Range Dykes[a]	620–610	19	355	18	34N–6S	Murthy et al. (1992), Kamo and Gower (1994)
	Callander complex	575 ± 5	−46	121	6	34S–81S	Symons and Chiasson (1991)
	Catochin Basalts-A	564 ± 9	−42	117	9	32S–77S	Meert et al. (1994)
	Sept-Iles complex B[b]	564 ± 4	−44	135	5	27S–74S	Tanczyk et al. (1987)
Siberia							
20	Karagas Series	850(?)–740	−12	97	10	22N–8N	Metelkin et al. (2005)
21	Nersinsky complex	~740	−37	122	11	2N–19S	Metelkin et al. (2005)
	Mean pole for V_{2edc}	~560	−35	77	6	3S–16S	Shatsillo et al. (2006)
	Redkolesnaya Fm.	~550	−61	68	5	30S–42S	Shatsillo et al. (2006)
	Mean pole for the Nemakit-Daldynian stage	~540	−60	115	7	25S–41S	Shatsillo et al. (2006)
	Mean pole for Cam_1	~525	−48	151	8	19S–36S	Shatsillo et al. (2006)
Baltica							
22	Hunnedalen dykes	~848	−41	222	10	59S–87S	Walderhaug et al. (1999)
	Egersund dykes	~608	−31	224	15	50S–81S	Walderhaug et al. (2007)
	Mean pole	~555	−30	298	10	4S–31S	Popov et al. (2002), Iglesia-Llanos et al. (2005), Popov et al. (2005)
	Tornetrask Formation	~535	−56	296	12	24S–52S	Torsvik and Rehnstrom (2001)

Comments: No, numbers of the results that are used in Fig. 8. Pole, coordinates of the north paleomagnetic pole: Φ, latitude (positive for northern hemisphere); Λ, longitude (east). A_{95}, radius of confidence circle around paleomagnetic pole. Lat, the range of paleolatitudes, which were occupied by a craton. *Abbreviations*: IND: India; SEY: Seychelles.

[a] Recalculated by Hodych et al. (2004).

[b] The Sept-Iles complex "B" direction (after correction for minor tilt – see Symons and Chiasson, 1991) matches other ~570 Ma poles from Laurentia, while "A" direction falls close to the Cambro-Ordovician segment of the North American APWP (see Meert et al., 1994).

[c] Estimated age based on stratigraphic information given in Pisarevsky et al. (2001) and stable isotope calibration given in Walter et al. (2000).

[d] Estimated age based on known isotopic and/or stratigraphic position.

[e] Rotated to India according to Torsvik et al. (2001b).

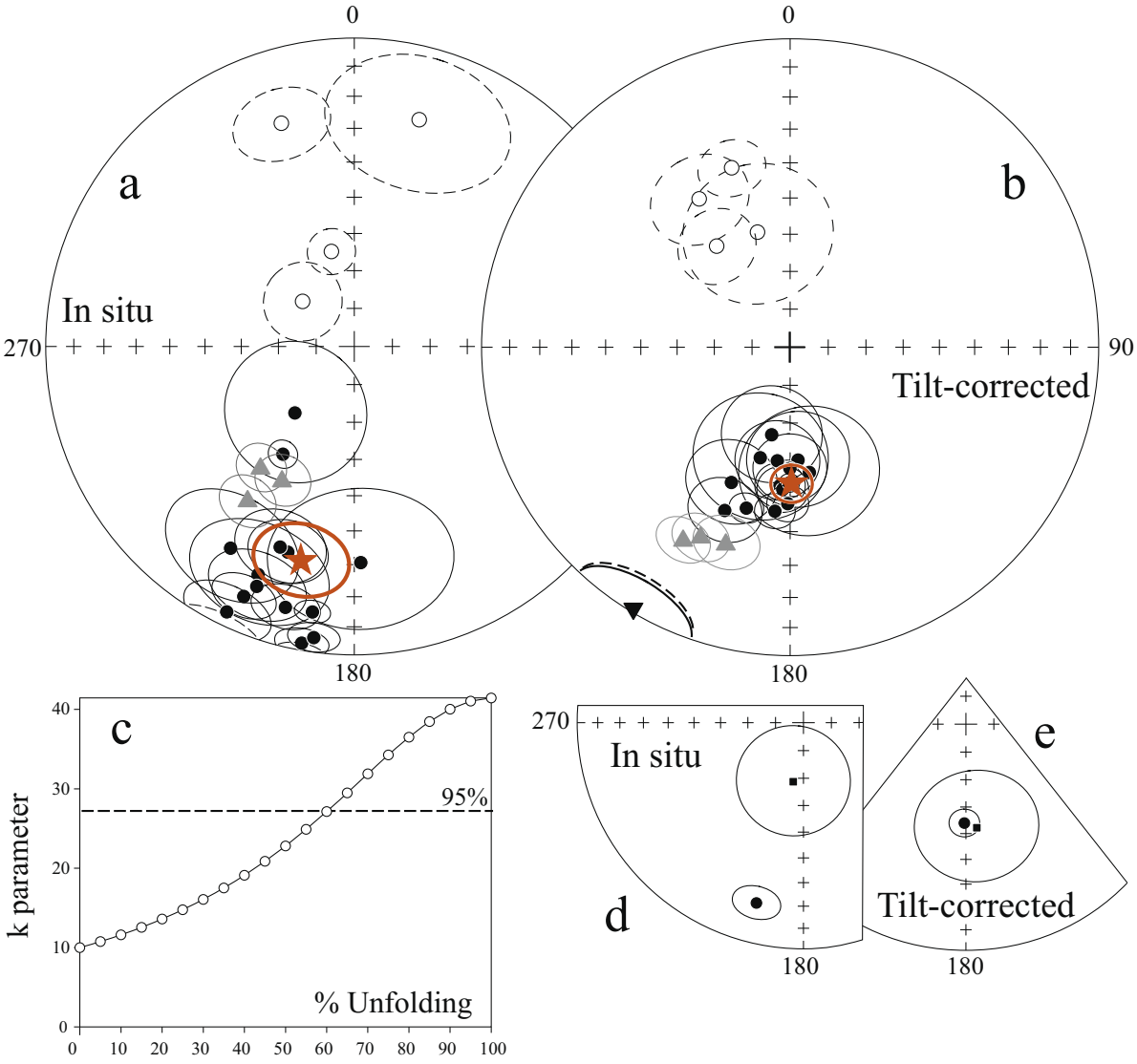

Fig. 7. (a and b) Stereoplots of HTC site-mean directions (circles) with confidence circles (thin lines) in situ (a) and after tilt correction (b). Star is the HTC overall mean with confidence circle (thick line). Shaded triangles are three discarded sites, where adequate component separation is not achieved (see text for discussion). Inverted triangle in b is the overall ITC mean. (c) Plot of concentration parameter for HTC site-means versus percent of unfolding. (d and e) Stereoplots of the HTC mean directions with confidence circles for sections A (circle) and B (square) in situ (d) and after tilt correction (e). Other notation is as in Fig. 6.

and the presence of a 750–800 Ma large felsic igneous province in Rajasthan invites comparisons to the similarly-aged volcanic sequences in the CAOB (Gregory et al., 2009; Meert et al., 2010; Pradhan et al., 2008).

It is possible to apply a combination of geologic and paleomagnetic "filters" in order to identify potential 'mother' plate(s) for the CAOB blocks. We know of no geologic evidence of connections between the CAOB microcontinents and future-West Gondwana cratons. Moreover, extracting these microcontinents "from under Laurentia" and moving them through the future-West Gondwana blocks requires an implausibly complicated trajectory to reach their Cambrian configuration. Therefore, we reject a southern hemispheric origin for the CAOB microcontinents.

We also note that irrespective of the polarity choice, Laurentia was positioned close to the equator and shows few, if any, geologic similarities to be regarded as the mother-plate for the CAOB microcontinents. Despite some geologic similarities between the CAOB microcontinents and Siberia for the late Neoproterozoic interval, paleolatitudes for Siberia at 770 Ma are also too low for placement adjacent to the CAOB and therefore we exclude Siberia from this list (Table 4, Fig. 8).

When examining the northern hemispheric option, India passes the paleomagnetic filter but the geologic comparisons are not as strong, whereas the situation is reversed for the North China craton. We propose that both can be excluded from the mother-plate list at the present time. Finally, Australia passes the paleomagnetic filter, but there are the above-noted uncertainties in stratigraphic correlations between Australia and the CAOB microcontinents (Chumakov, 2009b). The above discussion essentially leaves us with two options, either Tarim and/or South China, as potential mother plates for the Kazakhstan and Mongol domains. Either satisfies the paleomagnetic similarity for coeval paleolatitudes and both show strong geological correlations. Australia and India cannot be completely ruled out, but we consider them as less likely candidates.

Available data are insufficient to establish the timing of the Kazakhstan and Mongol domains separation from their mother-plate (plates?). However, the stratigraphic similarities between the late Neoproterozoic–early Cambrian sedimentary covers of the above listed plates and Kazakhstan and Mongol domains leaves us with two possibilities: (a) the domains did not separate from their mother-plate (plates?) until the Early Cambrian or (b) all

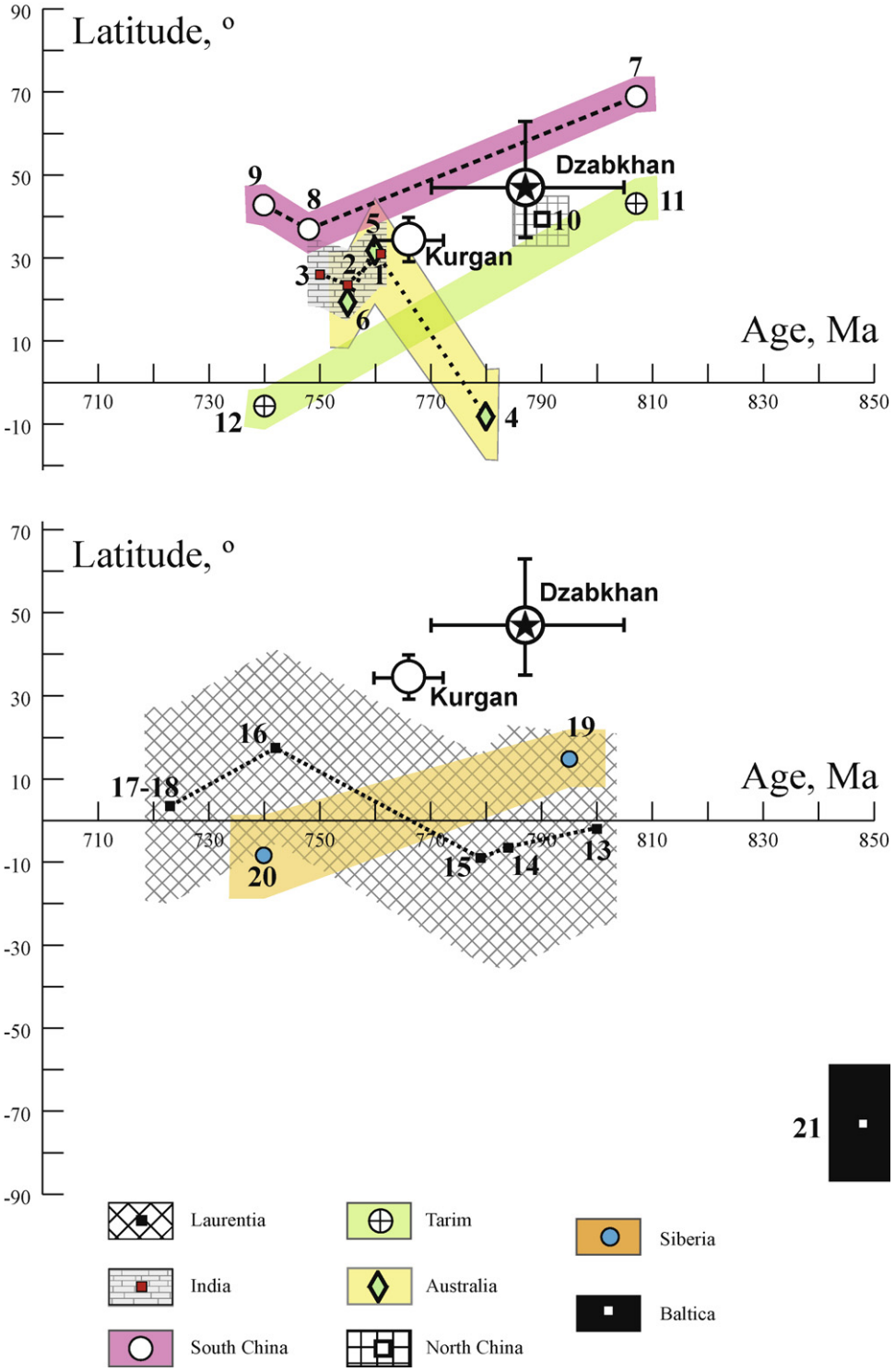

Fig. 8. Paleolatitude versus age plots for major cratons and the observed values for Kurgan tuffs of the Lesser Karatau microcontinent (asterisk) and the Dzabkhan volcanics (large encircled star with error bars) from Levashova et al. (2010). For major cratons, the symbols correspond to the paleolatitudes of their centers, while the corresponding bands denote the paleolatitude range covered by this craton (without error limits). If more than two points are available from a craton, the symbols are connected by thick dashed lines for better visibility. The data are numbered as in Table 4.

these landmasses were evolving under similar conditions in the late Neoproterozoic–early Cambrian.

Judged by the abundance of carbonates in the latest Neoproterozoic (ca. Ediacaran)–Early Cambrian, all these units were located in a shallow and warm sea. In terminal Neoproterozoic–Early Cambrian time, the paleomagnetic data for South China (Lin et al., 1985) and available paleomagnetic results from the Tuva-Mongolia, Lesser Karatau and Baydaric microcontinents (Kravchinsky et al., 2001, 2010; Pradhan et al., 2009) place the entire system at equatorial latitudes.

A lithological and geochemical study of latest Neoproterozoic–Cambrian sedimentary cover allowed Veshcheva et al. (2008) to reconstruct the provenance of clastic material in terrigenous rocks of the Tuva-Mongol massif. These authors con-

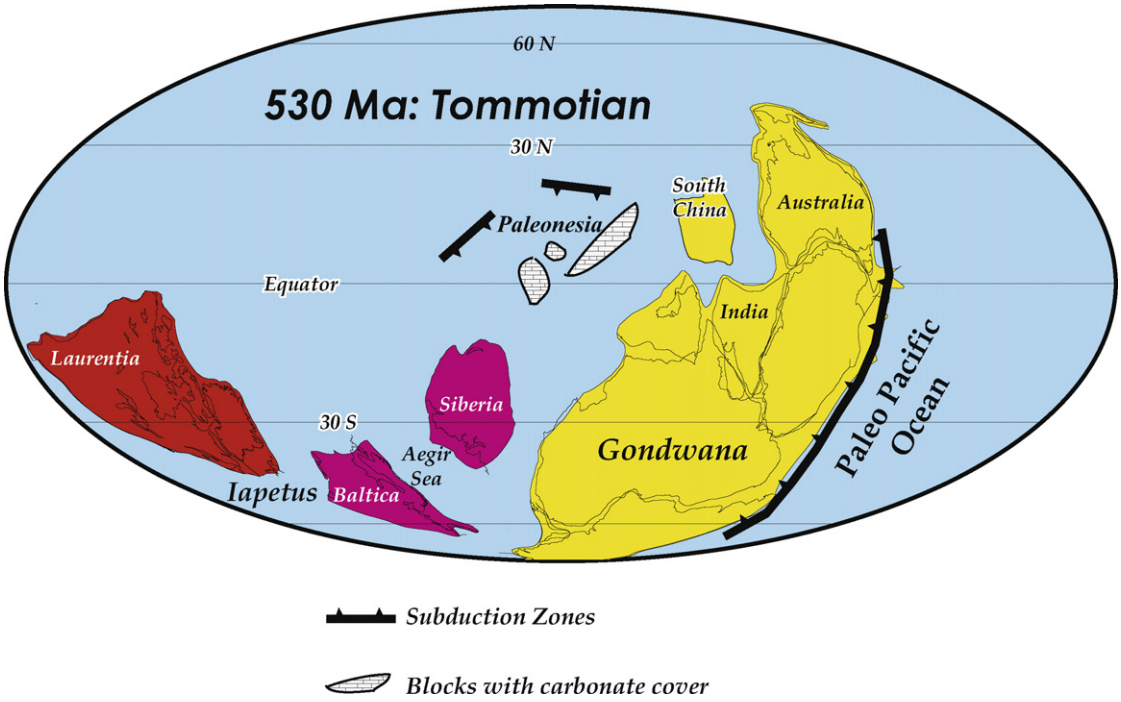

Fig. 9. Paleogeographic reconstruction for Tommotian time (simplified from Fig. 7 in Meert and Lieberman, 2008) showing provisional location of CAOB microcontinents with thick carbonate covers and surrounding island arcs.

cluded that plagioclase-dominated granitoids of the Gargan block were the main suppliers, with a smaller contribution from late Neoproterozoic ophiolites and island arc complexes. In contrast, a contribution from the early Precambrian crust of the Siberian craton was nearly absent. Thus, according to Veshcheva et al. (2008), the Tuva-Mongol composite massif was neither welded to, nor proximal to, Siberia. This conclusion is at directly at odds with recently published paleomagnetic data from Eastern Sayan (Kravchinsky et al., 2010) that were used to place Tuva-Mongolia adjacent to Siberia during the Cambrian.

In the Nemakit-Daldynian (ca. 542–530 Ma) and Tommotian (ca. 530–520 Ma), small shelly fossils from the coeval sections of Tarim, South China, and the Aldan part of Siberia as well as from several CAOB microcontinents have a number of similar taxa at the family, genus, and even species levels (Esakova and Zhegallo, 1996). In the Atdabanian and Botomian (ca. 520–512 Ma), Siberia, Tarim, South China, and the CAOB microcontinents belonged to the same trilobite province and were distinct from Australia (Repina, 1985; Meert and Lieberman, 2004). It is possible that trilobite spat were able to migrate between Siberia, Kazakzhstan, Tuva-Mongol, Tarim and South China in a relatively small equatorial ocean bordering these landmasses. The same is true for the first archaeocyathid reefs which had appeared in Siberia within the humid tropical zone in the Tommotian and reached Australia somewhat later in the middle of the Atdabanian (Zhuravleva, 1981; Meert and Lieberman, 2008). Repina (1985) suggested that small shelly fossils migrated between these continents in a similar fashion.

Subduction-related complexes are recognized indifferent parts of the CAOB. For instance, Ruzhentsev and Burashnikov (1995) described presumably Ediacaran–early Cambrian island arc complexes in the Lake zone of western Mongolia and tentatively traced these island arcs to the southeast of Tuva (Fig. 1b). The Selety island arc of Tommotian age in North Kazakhstan, the 1000-km-long Bozshakol-Chingiz island arc in East Kazakhstan that originated in the Atdabanian, and fragments of early Cambrian island arc complexes in South Kazakhstan (Degtyarev and Ryazantsev, 2007) are most probably parts of the same puzzle. Unfortunately, we cannot reconstruct the spatial relationship between the continental blocks and island arcs. However, the lack of a tuffaceous influx in the carbonates suggests that the continental blocks were likely distal from these now adjacent island arcs.

In an attempt to illustrate a much-generalized relationship between the cratons, microcontinents and island arcs, we have drawn the above-discussed tectonic unit on a scheme for the beginning of Cambrian time (Fig. 9) but must stress that this figure should not be considered as a reconstruction (i.e. something certain and well defined). An oceanic domain was probably located at equatorial latitudes to the north of Siberia. Following Chumakov (2009b), we have positioned the Tarim craton adjacent to the Kazakhstan domain but shown the Tuva-Mongol domain separately from either the South China or Tarim plates, in accord with the above evidence.

7. Conclusions

We report new paleomagnetic data and U–Pb zircon ages for Neoproterozoic volcano-sedimentary rocks from the Lesser Karatau block in central Kazakhstan. The LA-ICP-MS U–Pb zircon age of felsic tuffs of the Kurgan Fm. is 766 ± 7 Ma. At that time the Lesser Karatau microcontinent (central Kazakhstan) was located at a latitude of 34.2 ± 5.3°, N or S. The only other CAOB microcontinent for which paleomagnetic data are available (at ~770 Ma) is the Baydaric microcontinent in central Mongolia (Levashova et al., 2010). The LA-ICP-MS U–Pb zircon age of volcanic rocks of the Dzabkhan Fm. is 770–805 Ma. At that time, the Baydaric microcontinent was located at latitude of 47 ± 14°, N or S.

Several lines of evidence favor the view that CAOB microcontinents had originally been parts of two larger domains and allow us to extrapolate the use of our paleomagnetic data to a larger model of the Kazakhstan and Mongol domains. These domains may once have belonged to major cratonic areas. Our combined analysis of paleomagnetic, geologic, geochronologic and paleontologic data enabled us to exclude the southern hemisphere as a possible location of the CAOB microcontinents at 750–800 Ma. Of several cratons that were located in the northern hemisphere at that time

we favor a hypothesis that the Kazakhstan and Mongol domains had originally belonged either to Tarim or South China.

The available geological information indicates that a large, shallow, warm sea with an archipelago of continental blocks existed to the north of Siberia in the end of the Neoproterozoic–the beginning of the Paleozoic. We suggest that the Early Paleozoic "disposition" of the CAOB units could resemble the present-day Arctic Canada archipelago but surrounded by multiple subduction zones (Fig. 9).

Acknowledgments

We thank many colleagues from the Scientific Station of the Russian Academy of Sciences in Bishkek (Kyrgyzstan) for logistic support of the fieldwork. We would like to thank Kirill Degtyarev for helpful discussions and Alfred Kröner and an anonymous reviewer for instructive comments. This study was supported by the Division of Earth Sciences and the Office of International Science and Engineering's Eastern and Central Europe Program of the U.S. National Science Foundation, Grant EAR05-08597. Support was also derived from the Russian Foundation of Basic Research, Grant 07-05-00021, and Program no. 9 of the Earth Science Division, Russian Academy of Sciences.

References

Alexeiev, D.V., 1990. The sequence of the Caledonian deformations in the Lesser Karatau Ridge. Geology and Ore prospecting in Kazakhstan. Alma-Ata, 134–138 (in Russian).
Alexeiev, D.V., 1993. Tectonics of the Lesser Karatau. The PhD Thesis, Moscow University, Geological Department, 145 p. (in Russian).
Ankinovich, S.G., 1962. The Lower Paleozoic of the vanadium-rich Central Tien-Shan Basin and of the Central Kazakhstan west margin. Alma-Ata, 185 p. (in Russian).
Bazhenov, M.L., Klishevich, V.L., Tselmovich, V.A., 1995. Paleomagnetism of Permian red beds from south Kazakhstan: DRM inclination error or CRM shallowed directions? Geophys. J. Int. 120, 445–452.
Bazhenov, M.L., Collins, A.Q., Degtyarev, K.E., Levashova, N.M., Mikolaichuk, A.V., Pavlov, V.E., Van der Voo, R., 2003. Paleozoic northward drift of the North Tien Shan (Central Asia) as revealed by Ordovician and Carboniferous paleomagnetism. Tectonophysics 366, 113–141.
Belichenko, V.G., Letnikova, E.F., Geletii, N.K., 1999. Geology of carbonate rocks in the sedimentary cover of the Tuva-Mongolia Microcontinent. Dokl. Earth Sci. 364, 1–4.
Berzin, N.A., Dobretsov, N.L., 1994. Geodynamic evolution of Southern Siberia in Late Precambrian–Early Paleozoic time. In: Coleman, R.G. (Ed.), Reconstruction of the Paleoasian Ocean, Proc. 29th Intern Geol. Congr. Utrecht, VSP, pp. 53–70.
Burtman, V.S., 1999. Some problems of the Paleozoic tectonic reconstructions in Central Asia. Geotectonics 33, 103–112.
Chen, Y., Xu, B., Zhan, S., Li, Y.G., 2004. First mid-Neoproterozoic paleomagnetic results from the Tarim Basin (NW China) and their geodynamic implications. Precambrian Res. 133, 271–281.
Chumakov, N.M., 1978. Precambrian Tillites and Tilloides. Nauka, Moscow, 202 p. (in Russian).
Chumakov, N.M., 2009a. The Baykonurian glaciohorizon of the Late Vendian. Stratigr. Geol. Correl. 17, 373–383.
Chumakov, N.M., 2009b. Neoproterozoic glacial events in Eurasia. In: Gaucher, C., Sial, A.N., Halverson, G.P., Frimmel, H.E. (Eds.), Neoproterozoic–Cambrian Tectonics, Global Change and Evolution: A Focus on Southwestern Gondwana. Developments in Precambrian Geology, vol. 16. Elsevier, pp. 389–403.
Cogné, J.P., 2003. PaleoMac: a Macintosh application for treating paleomagnetic data and making plate reconstructions. Geochem. Geophys. Geosyst. 4 (1), 1007, doi:10.1029/2001GC000227.
Degtyarev, K.E., Ryazantsev, A.V., 2007. Cambrian arc – continent collision in the Paleozoides of Kazakhstan. Geotectonics 41 (1), 63–86.
Didenko, A.N., Mossakovsky, A.A., Pechersky, D.M., Ruzhentsev, S.V., Samygin, S.G., Kheraskova, T.N., 1994. Geodynamics of Paleozoic oceans of Central Asia. Russ. Geol. Geophys. (7-8), 59–75 (in Russian).
Eganov, E.A., Sovetov, Y.K., 1979. The Karatau Range as a Model of Phosphorite Accumulation. Nauka, Novosibirsk, 190 p. (in Russian).
Esakova, N.V., Zhegallo, E.A., 1996. The Biostratigraphy and Fauna of the Early Cambrian in Mongolia. Nauka, Moscow, 270 p. (in Russian).
Evans, D.A., Zhuravlev, A.Y., Budney, C.J., Kirschvink, J.L., 1996. Palaeomagnetism of the Bayan-Gol Formation, western Mongolia. Geol. Mag. 133, 487–496.
Evans, D.A.D., Li, Z.X., Kirschvink, J.L., Wingate, M.T.D., 2004. A high-quality mid-Proterozoic paleomagnetic pole from South China, with implications for an Australia – Laurentia connection at 755 Ma. Precambrian Res. 100, 213–234.
Fisher, R.A., 1953. Dispersion on a sphere. Proc. R. Soc. Lond. A 217, 295–305.
Gregory, L.C., Meert, J.G., Bingen, B.H., Pandit, M.K., Torsvik, T.H., 2009. Paleomagnetic and geochronologic study of Malani Ingeous suite, NW India: implications for the configuration of Rodinia and the assembly of Gondwana. Precambrian Res. 170, 13–26.
Hargraves, R.B., Duncan, R.A., 1990. Radiometric age and paleomagnetic results from Seychelles dikes. In: Duncan, R.A., et al. (Eds.), Proceedings of the Ocean Drilling Program. Scientific Results Leg, vol. 115, pp. 119–122.
Harlan, S.S., Geissman, J.W., Snee, L.W., 1997. Paleomagnetic and 40Ar/39Ar geochronologic data from Late Proterozoic mafic dykes and sills, Montana and Wyoming. USGS Professional Paper 1580, 16 pp.
Heaman, L.M., Le Cheminant, A.N., Rainbird, R.H., 1992. Nature and timing of Franklin igneous events, Canada – implications for a late Proterozoic mantle plume and the break-up of Laurentia. Earth Planet. Sci. Lett. 109, 117–131.
Hodych, J.P., Cox, R.A., Košler, J., 2004. An equatorial Laurentia at 550 Ma confirmed by Grenvillian inherited zircons dated by LAM ICP-MS in the Skinner Cove volcanics of western Newfoundland: implications for inertial interchange true polar wander. Precambrian Res. 129, 93–113.
Hoffman, P.F., 1991. Did the breakout of Laurentia turn Gondwanaland inside-out? Science 252, 1409–1412.
Horstwood, M.S.A., Foster, G.L., Parrish, R.R., Noble, S.R., Nowell, G.M., 2003. Common-Pb corrected in situ U–Pb accessory mineral geochronology by LA-MC-ICP-MS. J. Anal. At. Spectrom. 18, 837–846.
Huang, B.C., Xu, B., Zhang, C.X., Li, Y.A., Zhu, R.X., 2005. Paleomagnetism of the Baiyisi volcanic rocks (ca. 740 Ma) of Tarim Northwest China: a continental fragment of Neoproterozoic Western Australia? Precambrian Res. 142, 83–92.
Iglesia-Llanos, M.P., Tait, J.A., Popov, V., Ablamasova, A., 2005. Paleomagnetic data from Ediacaran (Vendian) sediments of the Arkhangelsk region, NW Russia: an alternative APWP of Baltica for the Late Proterozoic–Early Paleozoic. Earth Planet. Sci. Lett. 240, 732–747.
Kamo, S.L., Gower, C.F., 1994. Note: U–Pb baddeleyite dating clarifies age of characteristic paleomagnetic remanence of Long Range dykes, southeastern Labrador. Atl. Geol. 30, 259–262.
Khain, E.V., Neimark, L.A., Amelin, U.V., 1995. Caledonian stage of remobilization of the Gargan block basement, Eastern Sayan (isotopic geochronological data). Dokl. Earth Sci. 342, 776–780 (in Russian).
Khain, E.V., Bibikova, E.V., Salnikova, E.B., Kröner, A., Gibsher, A.S., Didenko, A.N., Degtyarev, K.E., Fedotova, A.A., 2003. The Palaeo-Asian ocean in the Neoproterozoic and early Palaeozoic: new geochronologic data and palaeotectonic reconstructions. Precambrian Res. 122, 329–358.
Kheraskova, T.N., Didenko, A.N., Bush, V.A., Volozh, Y.A., 2003. The Vendian-Early Paleozoic history of the continental margin of eastern Paleogondwana, Paleoasian Ocean, and Central Asian Foldbelt. Russ. J. Earth Sci. 5 (3), 165–184.
Khomentovsky, V.V., 1996. The Sinian system of China and its analogies in Siberia. Russ. Geol. Geophys. 37 (8), 136–153.
Khomentovsky, V.V., Fedorov, A.B., Karlova, G.A., 1998. The lower boundary of the Cambrian in the inner regions of the northern part of the Siberian platform. Stratigr. Geol. Correl. 6 (1), 3–11.
Kirschvink, J.L., 1978. The Precambrian Cambrian boundary problem; magnetostratigraphy of the Amadeus Basin, central Australia. Geol. Mag. 115, 139–150.
Kirschvink, J.L., 1980. The least-square line and plane and the analysis of palaeomagnetic data. Geophys. J. R. Astron. Soc. 62, 699–718.
Knipper, A.L., 1963. Tectonics of the Baykonur Synclinorium (Central Kazakhstan). Akademia Nauk SSSR, Moscow, 204 p. (in Russian).
Konnikov, E.G., Gibsher, A.S., Izokh, A.E., Skliarov, E.V., Khain, E.V., 1994. Late Precambrian evolution of the Paleoasian ocean northern segment: new radiological, geological and geochronological data. Russ. Geol. Geophys. (7–8), 152–168 (in Russian).
Kosler, J., Sylvester, P.J., 2003. Present trends and the future of zircon in geochronology: laser ablation ICPMS, Zircon. Rev. Mineral. Geochem. 53, 243–271.
Korolev, V.G., Maksumova, R.A., 1984. Precambrian Tillites and Tilloides of the Tien-Shan. Ilim, Frunze, 189 p. (in Russian).
Kozakov, I.K., Bibikova, E.V., Neymark, L.A., Kirnozova, T.I., 1993. The Baydaric block. In: Rudnik, B.A., Sokolov, Y.M., Filatova, L.I. (Eds.), Early Precambrian of the Central Asian Fold Belt. Nauka, St. Petersburg, pp. 118–137 (in Russian).
Kravchinsky, V.A., Konstantinov, K.M., Cogné, J.-P., 2001. Paleomagnetic study of Vendian and Early Cambrian rocks of South Siberia and Central Mongolia: was the Siberian platform assembled at this time? Precambrian Res. 110, 61–92.
Kravchinsky, V.A., Sklyarov, E.V., Gladkochub, D.B., Harbert, W.P., 2010. Paleomagnetism of the Precambrian Eastern Sayan rocks: implications for the Ediacaran–Early Cambrian paleogeography of the Tuva-Mongolian composite terrane. Tectonophysics 486, 65–80.
Kröner, A., Windley, B.F., Badarch, G., Tomurtogoo, O., Hegner, E., Jahn, B.M., Gruschka, S., Khain, E.V., Demoux, A., Wingate, M.T.D., 2007. Accretionary growth and crust formation in the Central Asian Orogenic Belt and comparison with the Arabian-Nubian shield. Geol. Soc. Am. Mem. 200, 181–209.
Kuzmichev, A.B., 1996. Riphean Ophiolites of the Kitoy Bald Mountains: structural setting and Obduction Age. Geol. Razvedka (3), 11–25 (in Russian).
Kuzmichev, A.B., 2004. Tectonic History of the Tuva-Mongol Massif: Early Baikalian, Late Baikalian and Early Caledonian Stages. PROBEL-2000, Moscow, 192 p. (in Russian).
Levashova, N.M., Kalugin, V.M., Gibsher, A.S., Yff, J., Ryabinin, A.B., Meert, J.G., Malone, S.J., 2010. The origin of the Baydaric Microcontinent, Mongolia: constraints from paleomagnetism and geochronology. Tectonophysics 485, 306–320.
Li, X.H., Li, Z.X., Zhou, H., Liu, Y., Kinny, P.D., 2002. U–Pb zircon geochronology, geochemistry and Nd isotopic study of Neoproterozoic bimodal volcanic rocks in the Kangdian Rift of South China; implications for the initial rifting of Rodinia. Precambrian Res. 113, 135–154.

Li, Z.X., Zhang, L., Powell, C.M., 1996. Positions of the East Asian cratons in the Neoproterozoic supercontinent Rodinia. Aust. J. Earth Sci. 43, 593–604.
Li, Z.X., 2000. New palaeomagnetic results from the "cap dolomite" of the Neoproterozoic Walsh Tillite, northwestern Australia. Precambrian Res. 100, 359–370.
Li, Z.X., Evans, D.A.D., Zhang, S., 2004. A 90° spin on Rodinia: possible causal links between the Neoproterozoic supercontinent, superplume, true polar wander and low-latitude glaciation. Earth Planet. Sci. Lett. 220, 409–421.
Li, Z.X., Bogdanova, S.V., Davidson, A., Collins, A.S., De Waele, B., Ernst, R.E., Fitzsimons, I.C.W., Fuck, R.A., Gladkochub, D.P., Jacobs, J., Karlstrom, K.E., Lu, S., Natapov, L.M., Pease, V., Pisarevsky, S.A., Thrane, K., Vernikovsky, V., 2008. Assembly, configuration, and break-up history of Rodinia: a synthesis. Precambrian Res. 160, 179–210.
Lin, J.L., Fuller, M.D., Zhang, W.Y., 1985. Paleogeography of the North and South China blocks during the Cambrian. J. Geodyn. 2, 91–114.
Lu, S., Zhao, G., Wang, H., Hao, G., 2008. Precambrian basement and sedimentary cover of the North China Craton: a review. Precambrian Res. 160, 77–93.
Ludwig, K.R., 2004. Users manual for ISOPLOT, a geochemical toolkit for Microsoft Excel version 3.09a.
Mambetov, A.M., Repina, L.N., 1979. The Lower Cambrian of the Talas Ala-too and its correlation with the sections of the Lesser Karatau and the Siberian platform. In: Zhuravleva, I.T., Meshkova, N.P. (Eds.), Biostratigraphy and Paleontology of the Lower Cambrian of the Siberian Platform. Nauka, Novosibirsk, pp. 98–138 (in Russian).
Mardia, K.V., 1972. Statistics of Directional Data. Academic Press, London, 357 p.
McElhinny, M.W., 1964. Statistical significance of the fold test in palaeomagnetism. Geophys. J. R. Astron. Soc. 8, 338–340.
McFadden, P.L., Jones, D.L., 1981. The fold test in palaeomagnetism. Geophys. J. R. Astron. Soc. 67, 53–58.
McFadden, P.L., McElhinny, M.W., 1988. The combined analysis of remagnetization circles and direct observations in palaeomagnetism. Earth Planet. Sci. Lett. 87, 161–172.
McFadden, P.L., McElhinny, M.W., 1990. Classification of the reversal test in palaeomagnetism. Geophys. J. Int. 103, 725–729.
McWilliams, M.O., McElhinny, M.W., 1980. Late Precambrian paleomagnetism in Australia: the Adelaide Geosyncline. J. Geol. 88, 1–26.
Meert, J.G., Van der Voo, R., Payne, T., 1994. Paleomagnetism of the Catoctin volcanic province: a new Vendian–Cambrian apparent polar wander path for North America. J. Geophys. Res. 99 (B3), 4625–4641.
Meert, J.G., Gibsher, A.S., Levashova, N.M., Grice, W.C., Kamenov, G.D., Rybanin, A. Glaciation and 770 Ma Ediacaran (?) fossils from the Lesser Karatau microcontinent, Kazakhstan. Gondwana Res., doi:10.1016/j.gr.2010.11.008.
Meert, J.G., Pandit, M.K., Pradhan, V.R., Banks, J., Sirianni, R., Stroud, M., Newstead, B., Gifford, J., 2010. Precambrian crustal evolution of Peninsular India: a 3.0 billion year odyssey. J. Asian Earth Sci. 39, 483–515.
Meert, J.G., 2003. A synopsis of events related to the assembly of eastern Gondwana. Tectonophysics 362, 1–40.
Meert, J.G., Torsvik, T.H., 2003. The making and unmaking of a supercontinent: Rodinia revisited. Tectonophysics 375, 261–288.
Meert, J.G., Torsvik, T.H., 2004. Reply to J.D.A. Piper: the making and unmaking of a supercontinent: Rodinia revisited. Tectonophysics 383, 99–103.
Meert, J.G., Lieberman, B.S., 2004. A palaeomagnetic and palaeobiogeographical perspective on latest Neoproterozoic and early Cambrian tectonic events. J. Geol. Soc. Lond. 161, 477–487.
Meert, J.G., Lieberman, B.S., 2008. The Neoproterozoic assembly of Gondwana and its relationship to the Ediacaran–Cambrian radiation. Gondwana Res. 14, 5–21.
Metelkin, D.V., Belonosov, I.V., Gladkochub, D.P., Donskaya, T.V., Mazukabzov, A.M., Stanevich, A.M., 2005. Paleomagnetic directions from Nersa intrusions of the Birusa terrane, Siberian craton as a reflection of tectonic events in the Neoproterozoic. Russ. Geol. Geophys. 46, 395–410 (in Russian).
Missargevsky, V.V., Mambetov, A.M., 1981. Stratigraphy and Fauna of the Boundary Layers of Cambrian and Precambrian in the Lesser Karatau. Nauka, Moscow, 92 p. (in Russian).
Mossakovsky, A.A., Ruzhentsev, S.V., Samygin, S.G., Kheraskova, T.N., 1993. The Central Asian fold belt: geodynamic evolution and formation. Geotectonics 27 (6), 3–32.
Murthy, G., Gower, C., Tubrett, M., Patzold, R., 1992. Paleomagnetism of Eocambrian Long Range dykes and Double Mer Formation from Labrador Canada. Can. J. Earth Sci. 29, 1224–1234.
Paces, J.B., Miller Jr., J.D., 1993. Precise U–Pb ages of Duluth complex and related mafic intrusions, Northeastern Minnesota: Geochronological insights to physical, petrogenetic, paleomagnetic, and tectonomagmatic processes associated with the 1.1 Ga midcontinent rift system. J. Geophys. Res. 98, 13997–14013.
Palmer, H.C., Baragar, W.R.A., Fortier, M., Foster, J.H., 1983. Paleomagnetism of Late Proterozoic rocks, Victoria Island, Northwest Territories, Canada. Can. J. Earth Sci. 20, 1456–1469.
Park, J.K., 1994. Palaeomagnetic constraints on the position of Laurentia from middle Neoproterozoic to Early Cambrian times. Precambrian Res. 69, 95–112.
Park, J.K., Norris, D.K., Larochelle, A., 1989. Paleomagnetism and the origin of the Mackenzie Arc of northwestern Canada. Can. J. Earth Sci. 26, 2194–2203.
Pidgeon, R.T., Smith, C.B., Fanning, C.M., 1989. Kimberlite and lamproite emplacement ages in Western Australia. In: Ross, J., et al. (Eds.), Kimberlites and Related Rocks, Volume 1: Their Composition, Occurrence, Origin and Emplacement. Blackwell Scientific Publications, Carlton, pp. 382–391 (Geol. Soc. Aust. Special Publication).
Pisarevsky, S.A., Li, Z.X., Grey, K., Stevens, M.K., 2001. A palaeomagnetic study of Empress 1A, a stratigraphic drillhole in the Officer Basin: evidence for a low-latitude position of Australia in Neoproterozoic. Precambrian Res. 110, 93–108.
Pisarevsky, S.A., Wingate, M.T.D., Stevens, M.K., Haines, P.W., 2007. Paleomagnetic results from the Lancer-1 stratigraphic drill hole, Officer Basin, Western Australia, and implications for Rodinia reconstructions. Aust. J. Earth Sci. 54, 561–572.
Popov, V., Iosifidi, A., Khramov, A., Tait, J., Bachtadze, V., 2002. Paleomagnetism of Upper Vendian sediments from the Winter Coast, White Sea region, Russia: implications for the paleogeography of Baltica during Neoproterozoic times. J. Geophys. Res. 107, 2315.
Popov, V., Khramov, A., Bachtadze, V., 2005. Paleomagnetism, magnetic stratigraphy and petromagnetism of the Upper Vendian sedimentary rocks in the sections of the Zolotitsa River and in the Verkhotina Hole, Winter Coast of the White Sea, Russia. Russ. J. Earth Sci. 7, 1–29.
Pradhan, V.R., Meert, J.G., Levashova, N.M., Gibsher, A.S., 2009. Preliminary paleomagnetic data on Late Cambrian to Ordovician carbonate beds of Tamdy Series from the Lesser Karatau microcontinent, South Kazakhstan. Geol. Soc. Am. 7, 269 (abstracts 41).
Pradhan, V.R., Meert, J.G., Pandit, M.K., Kamenov, G., Gregory, L.C., Malone, S.J., 2008. India's changing place in global Proterozoic reconstructions: new geochronologic constraints on key paleomagnetic poles from the Dharwar and Aravalli/Bundelkhand cratons. J. Geodyn. 50, 224–242.
Puchkov, V.N., 2000. Paleogeodynamics of the Southern and Middle Urals. Dauria, Ufa, 146 p. (in Russian).
Repina, L.N., 1985. The Paleobiogeography of the Early Cambrian seas based on trilobites. In: Khomentovsky, V.V. (Ed.), Biostratigraphy and Biogeography of the Paleozoic in Siberia. Academy of Sciences, Novosibirsk, pp. 5–15 (in Russian).
Rui, Z.Q., Piper, J.D.A., 1997. Paleomagnetic study of Neoproterozoic glacial rocks of the Yangtze Block; paleolatitudes and configuration of South China in the late Proterozoic supercontinent. Precambrian Res. 85, 173–199.
Ruzhentsev, S.V., Burashnikov, V.V., 1995. The tectonics of the Western Mongolia Salairides. Geotectonics 29 (5), 25–40.
Sengör, A.M.C., Natal'in, B.A., 1996. Paleotectonics of Asia: fragments of a synthesis. In: Yin, A., et al. (Eds.), The Tectonic Evolution of Asia. Cambridge University Press, Cambridge, pp. 486–640.
Shanker, R., Bhattacharya, D.D., Pande, A.C., Mathur, V.K., 2004. Ediacaran biota from the Jarashi (Middle Krol) and Mahi (Lower Krol) Formations, Krol Group, Lesser Himalaya, India. J. Geol. Soc. India 63, 649–654.
Shatsillo, A.V., Didenko, A.N., Pavlov, V.E., 2006. Paleomagnetism of Vendian Deposits of the Southwestern Siberian Platform. Russ. J. Earth Sci. 8, ES2003, doi:10.2205/2005ES000182.
Simonetti, A., Heaman, L.M., Hartlaub, R.P., Creaser, R.A., MacHattie, T.G., Bohm, C., 2005. U–Pb zircon dating by laser ablation-MC-ICP-MS using a new multiple ion counting Faraday collector array. J. Anal. At. Spectrosc. 20, 677–686.
Sohl, L.E., Christie-Blick, N., Kent, D.V., 1999. Paleomagnetic polarity reversals in Marinoan (ca 600 Ma) glacial deposits of Australia: implications for the duration of low-latitude glaciation in Neoproterozoic time. Geol. Soc. Am. Bull. 111, 1120–1139.
Sovetov, Y.K., 1990. The Precambrian–Cambrian Boundary and Precambrian Sedimentary Assemblages in the Lesser Karatau: Stratigraphic, Sedimentologic and Paleotectonic Aspects. Russian Academy of Sciences, Novosibirsk, Preprint #14, 36 p. (in Russian).
Stampfli, G.M., Borel, G.D., 2002. A plate tectonic model for the Paleozoic and Mesozoic constrained by dynamic plate boundaries and restored synthetic oceanic isochrones. Earth Planet. Sci. Lett. 196, 17–33.
Symons, D.T.A., Chiasson, A.D., 1991. Paleomagnetism of the Callander Complex and the Cambrian apparent polar wander path for North America. Can. J. Earth Sci. 28, 355–363.
Tanczyk, E.I., Lapointe, P., Morris, W.A., Schmidt, P.W., 1987. A paleomagnetic study of the layered mafic intrusions at Sept-Iles, Quebec. Can. J. Earth Sci. 24, 1431–1438.
Torsvik, T.H., Carter, L.M., Ashwal, L.D., Bhushan, S.K., Pandit, M.K., Jamtveit, B., 2001a. Rodinia refined or obscured: palaeomagnetism of the Malani igneous suite (NW India). Precambrian Res. 108, 319–333.
Torsvik, T.H., Ashwal, L.D., Tucker, R.D., Eide, E.A., 2001b. Neoproterozoic geochronology and palaeogeography of the Seychelles microcontinent: the India link. Precambrian Res. 110, 47–59.
Torsvik, T.H., Rehnstrom, E.F., 2001. Cambrian paleomagnetic data from Baltica: implications for true polar wander and Cambrian paleogeography. J. Geol. Soc. Lond. 158, 321–329.
Torsvik, T.H., Cocks, L.R.M., 2005. Norway in space and time: a Centennial cavalcade. Norwegian J. Geol. 85, 73–86.
Van der Voo, R., Levashova, N.M., Skrinnik, L.S., Kara, T.V., Bazhenov, M.L., 2006. Late orogenic, large-scale rotations in the Tien Shan and adjacent mobile belts in Kyrgyzstan and Kazakhstan. Tectonophysics 426, 335–360.
Veshcheva, S.V., Turkina, O.M., Letnikova, E.F., Ronkin, Y.L., 2008. Geochemical and Sm–Nd isotopic characteristics of the Neoproterozoic terrigenous rocks of the Tuva-Mongol massif. Dokl. Earth Sci. 418, 155–160.
Walderhaug, H.J., Torsvik, T.H., Eide, E.A., Sundvoll, B., Bingen, B., 1999. Geochronology and paleomagnetism of the Hunnedalen dykes, SW Norway: implications for the Sveconorwegian apparent polar wander loop. Earth Planet. Sci. Lett. 169, 71–83.
Walderhaug, H.J., Torsvik, T.H., Halvorsen, E., 2007. Geomagnetism, rock magnetism and palaeomagnetism. The Egersund dykes (SW Norway): a robust Early Ediacaran (Vendian) palaeomagnetic pole from Baltica. Geophys. J. Int. 168, 935–948.

Walter, M.R., Veevers, J.J., Calver, C.R., Gorjan, P., Hill, A.C., 2000. Dating the 840–544 Ma Neoproterozoic interval by isotopes of strontium, carbon and sulfur in seawater, and some interpretative models. Precambrian Res. 100, 371–432.

Weil, A.B., Geissman, J.W., Van der Voo, R., 2004. Paleomagnetism of the Neoproterozoic Chuar Group, Grand Canyon Supergroup, Arizona: implications for Laurentia's Neoproterozoic APWP and Rodinia break-up. Precambrian Res. 129, 71–92.

Williams, I.S., 1998. U–Th–Pb geochronology by ion microprobe. In: McKibben, M.A., Shanks III, W.C., Ridley, W.I. (Eds.), Applications of Microanalytical Techniques to Understanding Mineralizing Processes. Rev. Econ. Geol. 7, 1–35.

Windley, B.P., Alexeiev, D.V., Xiao, W., Kröner, A., Badarch, G., 2007. Tectonic models for accretion of the Central Asian Orogenic Belt. J. Geol. Soc. Lond. 164, 31–47.

Wingate, M.T.D., Giddings, J.W., 2000. Age and paleomagnetism of the Mundine Well dyke swarm, western Australia: implications for an Australia – Laurentia connection at 750 Ma. Precambrian Res. 100, 335–357.

Xiao, S.H., Bao, H.M., Wang, H.F., Kaufman, A.J., Zhou, C.M., Li, G.X., Yuan, X.L., Ling, H.F., 2004. The Neoproterozoic Quruqtagh Group in eastern Chinese Tianshan: evidence for a post-Marinoan glaciation. Precambrian Res. 130, 1–26.

Yakubchuk, A., Cole, A., Seltmann, R., Shatov, V.V., 2002. Tectonic Setting, Characteristics, and Regional Exploration Criteria for Gold Mineralization in the Altaid Tectonic Collage: The Tien Shan Province as a Key Example, vol. 9. Society of Economic Geologists, pp. 177–201 (Special Publications).

Yakubchuk, A., 2008. Re-deciphering the tectonic jigsaw puzzle of northern Eurasia. J. Asian Earth Sci. 32, 82–101.

Zhang, S., Li, Z.X., Wu, H., 2006. New Precambrian palaeomagnetic constraints on the position of the North China Block in Rodinia. Precambrian Res. 144, 213–238.

Zhao, G.C., Cao, L., Wilde, S.A., Sun, M., Li, S.Z., 2006. Implications based on the first SHRIMP U–Pb zircon dating on Precambrian granitoid rocks in North Korea. Earth Planet. Sci. Lett. 251, 365–379.

Zhuravleva, I.T., 1981. Paleobiogeography of the Early Cambrian, Paleontology, Paleobiogeography and Plate Tectonic Concept. SVNIMS, Magadan, pp. 43–51 (in Russian).

Zonenshain, L.P., Kuzmin, M.I., Natapov, L.M., Geology of the USSR: A Plate-Tectonic Synthesis. American Geophysical Union, Washington, D.C., Geodynamics Series 21, 1990, 242 p.

Zijderveld, J.D.A., 1967. AC demagnetization of rocks: analysis of results. In: Collinson, D.W., et al. (Eds.), Methods in Paleomagnetism. Elsevier, Amsterdam, pp. 254–286.

Zubtsov, E.L., 1971. Late Precambrian Ulutau – Tien-Shan Tillite Complex. Moscow State University, Moscow, 150 p. (in Russian).